

IKSPARK: An Inverse Kinematics Solver using Semidefinite Relaxation and Rank Minimization

Liangting Wu and Roberto Tron

Abstract—Inverse kinematics (IK) is a fundamental problem frequently occurred in robot control and motion planning. However, the problem is nonconvex because the kinematic map between the configuration and task spaces is generally nonlinear, which makes it challenging for fast and accurate solutions. The problem can be more complicated with the existence of different physical constraints imposed by the robot structure. In this paper, we develop an inverse kinematics solver named IKSPARK (Inverse Kinematics using Semidefinite Programming And Rank minimization) that can find solutions for robots with various structures, including open/closed kinematic chains, spherical, revolute, and/or prismatic joints. The solver works in the space of rotation matrices of the link reference frames and involves solving only convex semidefinite problems (SDPs). Specifically, the IK problem is formulated as an SDP with an additional rank-1 constraint on symmetric matrices with constant traces. The solver first solves this SDP disregarding the rank constraint to get a start point and then finds the rank-1 solution iteratively via a rank minimization algorithm with proven local convergence.

Compared to other work that performs SDP relaxation for IK problems, our formulation is simpler, and uses variables with smaller sizes. We validate our approach via simulations on different robots, comparing against a standard IK method.

I. INTRODUCTION

Over decades, robot manipulators have gained wide applications in areas such as manufacturing, medical surgeries, and aerospace. A fundamental problem for robots in these settings is inverse kinematics (IK) [22], where one needs to determine the values of the joint configurations that result in a given desired position and orientation of the end-effector.

Despite its importance, solving such problem is difficult for multiple reasons: 1) the kinematic map from joint angles to end-effector poses is generally nonlinear; 2) different numbers of solutions (zero, multiple distinct, or infinite) may exist depending on the structure of the robot and the query pose; 3) typically there are nonlinear equality and nonlinear constraints deriving from joint limits, self-intersection constraints, and closed kinematic chains.

In this paper we propose an IK solver named IKSPARK (Inverse Kinematics using Semidefinite Programming And Rank minimization). Instead of using joint angles, we parameterize the robot inverse kinematics problem over the set of rotation matrices $\text{SO}(3)$. We show that, by using this parameterization, we can write the kinematic constraints of the robot as convex constraints of rotation matrices. To overcome the nonlinearity brought by the manifold $\text{SO}(3)$, we introduce

a semidefinite relaxation of the kinematic constraints followed by a rank minimization algorithm.

The main contributions of this work are as follows:

- We parametrize the problem as a function of the rotation of reference frames of each link, allowing us to easily incorporate a variety of constraints and arrangements of links, covering:
 - spherical joints;
 - revolute joints with and without angle limits;
 - prismatic joints;
 - open/closed kinematic chains.
- We develop a relaxation of the manifold of robot configurations as a combination of linear and semidefinite constraints. Notably, we show that our relaxation is convex, it contains every kinematically feasible solution, and is tight in the sense that every kinematically feasible solution is on the boundary of the relaxed set. Moreover, we can use the relaxation as a sound method to check for kinematic feasibility.
- The total number of variables is linear to the number of joints; specifically, we use a 4×4 PSD (positive semidefinite) matrix for each revolute joint and a 8×8 PSD matrix for each prismatic joint. This is in contrast to other work using a single matrix whose total number of entries grows quadratically with the number of links.
- We propose a novel rank minimization algorithm to project any solution of the relaxed problem to a solution in the original IK problem. The algorithm is based on the maximization of the maximum eigenvalue of matrices with fixed trace over the relaxed set. We provide local convergence guarantees, and we show that, if the algorithm converges to a rank-one solution, then it will exactly satisfy all the constraints of the original IK problem (including the $\text{SO}(3)$ rotation constraints).

With respect to our preliminary work in [25], we include prismatic joints, use of quaternions to reduce the number of variables, and an alternative rank minimization approach for problems with uncertain minimal costs.

II. RELATED WORK

Previous work has shown that a finite number of analytical solutions for manipulators with up to 6-DOF exist [12], and can be derived in algebraic form [9], [20]. The popular solver IKFast [5] generalizes this method and automatically computes IK solutions in closed form. However, analytical methods are generally unavailable for robots with higher DOFs. On the other hand, numerical methods have been

The authors are with Department of Mechanical Engineering, Boston University, 110 Cummington Mall, Boston, MA 02215, USA. Emails: tomwu@bu.edu, tron@bu.edu The authors gratefully acknowledge the support by NSF award FRR-2212051.

successful in solving the IK problem, producing numerous efficient inverse-kinematics solvers such as CCD [10], triangulation [17] and FABRIK [1]. These solvers often perturb joint angles iteratively to decrease a distance between the end-effector and the target. Despite their efficiency, kinematic constraints such as self-collision, multiple end-effectors, and closed chains are either ignored or require ad-hoc modifications.

Other approaches to IK are based on formulations as nonlinear optimization problems which are then solved numerically, such as in [3], [11]. The main weakness of these methods is that, in general, there is no guarantee that the global optimum can be reached from arbitrary initial conditions. Moreover, it becomes difficult to enforce constraints deriving from closed kinematic chains.

Instead of solving nonlinear problems directly, some other work relaxes the nonlinear constraints and solves an approximated IK problem. To name a few, Dai et al. [4] introduce an IK solver based on mixed-integer convex optimization and can certify global infeasibility. Maric et al. [15] use a Riemannian manifold parameterization to enable solutions with mature Riemannian optimization methods. Similar to our approach, [29] and [7] both relax the IK problem into semidefinite problems (SDPs) each with an additional low-rank constraint. Different parameterizations are used in these two work. The former uses global rigid body transformations while the latter uses a “distance-geometric” formulation. In these two papers, the rank constraints are treated differently, where [29] drops the constraint for convex relaxation while [7] provides a rank minimization algorithm. Compared to [29], our approach uses a simpler formulation and has smaller dimension and, unlike [29], the rotations in our results are very close to actual rotations on $\mathbf{SO}(3)$ and do not require projections to $\mathbf{SO}(3)$ as a post-process. Compared to [7], our method parameterizes the robot differently and has a more principled rank minimization algorithm based on the maximization of the eigenvalues of positive semidefinite matrices with constant traces. In addition, we show that our method converges locally to feasible solutions.

Some other work also investigates semidefinite relaxation of problems not limited to IK, but general problems with rotations. For instance, [13], [26]–[28] propose SDP relaxations to different estimation problems involving rotations. In [2], [18], [21], the semidefinite relaxation techniques for such problems are evaluated for their tightness.

III. PRELIMINARIES

In this section we define some notation and derivations to be used in the rest of the paper.

A. General notation

We use \mathbf{I}_d to denote the identity matrix of dimension d , and we use \mathbf{e}_i to define a standard basis column vector with 1 in the i -th entry and zero elsewhere. We denote the set of $n \times n$ symmetric matrices as \mathbb{S}^n and the set of $n \times n$ positive semidefinite matrices as \mathbb{S}_+^n . For a matrix \mathbf{M} , we denote

$\mathbf{M}(a_1 : a_2, b_1 : b_2)$ as the block of entries in \mathbf{M} covering the a_1 -th to a_2 -th rows and b_1 -th to b_2 -th columns.

We make use of the vectorization property of the Kronecker product \otimes : $(\mathbf{B}^\top \otimes \mathbf{A})\text{vec}(\mathbf{X}) = \text{vec}(\mathbf{A}\mathbf{X}\mathbf{B})$, for any \mathbf{A} , \mathbf{B} and \mathbf{X} of appropriate dimensions.

B. Differentiating eigenvalues

Section VII-C introduced a rank minimization that uses the gradient of an eigenvalue with respect to the entries of the corresponding matrix. Specifically, consider a matrix $\mathbf{A} \in \mathbb{S}^n$, and let the eigenvalues of \mathbf{A} be $\lambda_1 > \dots > \lambda_n$. We are interested in finding $\frac{\partial \lambda_l}{\partial \mathbf{A}}$, for the l -th largest eigenvalue λ_l . Lemma 1 summarizes a result from [14, Theorem 1] (see that paper for a proof).

Lemma 1 (Gradient of eigenvalues): Given $\mathbf{X}_0 \in \mathbb{S}^n$, let \mathbf{v}_l and λ_l be a pair of *normalized* eigenvector and eigenvalue of \mathbf{X}_0 . For functions $\lambda(\mathbf{X}_0) = \lambda_l$ and $v(\mathbf{X}_0) = \mathbf{v}_l$ defined on neighborhood $\mathbf{X} = N(\mathbf{X}_0) \subset \mathbb{R}^{n \times n}$ of \mathbf{X}_0 , the gradient of $\lambda(\mathbf{X})$ is given by

$$\frac{\partial \lambda}{\partial \mathbf{X}} = \mathbf{v}_l \otimes \mathbf{v}_l. \quad (1)$$

Lemma 2: Under the same settings of Lemma 1, the largest eigenvalue as a function $\lambda_1(\mathbf{X})$ is convex in \mathbf{X} .

Proof: It is easy to see that for every \mathbf{v} the function $f(\mathbf{X}) = \mathbf{v}^\top \mathbf{X} \mathbf{v}$ is convex in \mathbf{X} and therefore $\lambda_1(\mathbf{X}) = \sup_{\|\mathbf{v}\|_2=1} \mathbf{v}^\top \mathbf{X} \mathbf{v}$ is convex in \mathbf{X} . ■

IV. PARAMETERIZATION

This section discusses how to model general kinematic chains using rotations and translations.

A. Kinematic chains

To create a model for the IK problem, we define a world inertial frame \mathcal{W} , and we associate a reference frame \mathcal{B}_i , $i \in \{1, \dots, n\}$ in correspondence of each joint. For revolute joints, the z -axis of each reference frame is aligned with the revolute axis.

We construct a graph $G = (\mathcal{V}, \mathcal{E})$, where \mathcal{V} is a set of indices for the links and \mathcal{E} is a set of ordered pairs that indicates the relations among the links. In particular, we have $(i, j) \in \mathcal{E}, i, j \in \mathcal{V}$ if the link i is the parent of link j . For robot with only spherical, revolute joints, and prismatic joints, \mathcal{E} has three disjoint subsets, $\mathcal{E}_s, \mathcal{E}_r$, and \mathcal{E}_p , respectively, representing the relations among spherical, revolute joints, and prismatic joints.

We define respectively \mathcal{V}_t and \mathcal{V}_r the subsets of \mathcal{V} whose translations and rotations are to be determined. We denote some subscripts, including *base* to represent a base frame (i.e., a frame rigidly attached to \mathcal{W}) and *ee* to represent the end-effector. We assume that there exists a path from any *base* = p_1 to the end effector *ee* = p_n , given by $\mathcal{P}_{fk} = \{p_1, p_2, \dots, p_n\} \subseteq \mathcal{V}$, where $(p_i, p_{i+1}) \in \mathcal{E}, \forall p_i, p_{i+1} \in \mathcal{P}_{fk}$.

B. Modeling kinematic chains using rotations and translations

The poses $\{\mathbf{R}_i, \mathbf{T}_i\}$ represent the rigid body transformation (rotation and translation) from the reference frame \mathcal{B}_i to the world frame, i.e., $\mathbf{R}_i = {}^W\mathbf{R}_{\mathcal{B}_i}$ and $\mathbf{T}_i = {}^W\mathbf{T}_{\mathcal{B}_i}$. To simplify the notation, we denote the relative rotation from \mathcal{B}_j to \mathcal{B}_i , ${}^{\mathcal{B}_i}\mathbf{R}_{\mathcal{B}_j}$ as ${}^i\mathbf{R}_j$, and the relative translation ${}^{\mathcal{B}_i}\mathbf{T}_{\mathcal{B}_j}$ as ${}^i\mathbf{T}_j$.

In this paper, we assign a reference frame \mathcal{B}_i to each link and parameterize our problem on subsets of $\{\mathbf{R}_i, \mathbf{T}_i\}$. This parameterization allows us to derive linear or semidefinite constraints, as we discuss in Section VII.

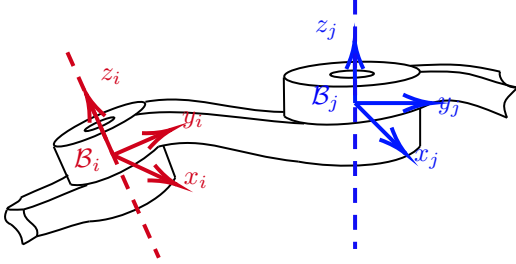


Fig. 1: Two connected links $(i, j) \in \mathcal{E}_r$, each associated with a reference frame (\mathcal{B}_i and \mathcal{B}_j).

A general set of variables to be solved for the IK problem is

$$\mathbf{x} = \{\mathbf{T}_i \in \mathbb{R}^3, \mathbf{R}_j \in \mathbf{SO}(3) | i \in \mathcal{V}_t, j \in \mathcal{V}_r\}. \quad (2)$$

We denote as n_t and n_r , respectively, the number of free translations and rotations in \mathbf{x} . We denote n_p as the number of prismatic joints.

V. KINEMATIC CONSTRAINTS

In this section we discuss how to model translation constraints on connected links as *linear* equality constraints and then investigate revolute joints and develop *linear* constraints on the joint axes and angle limits. In the end, we discuss the kinematic constraint on prismatic joints and how to develop the translation constraints on them.

A. Joint translations

Given the rigid structure of the robot, the relative translation between two reference frames on connected links (i, j) is fixed. For $(i, j) \in \mathcal{E}$, the following relation holds:

$$\mathbf{T}_j - \mathbf{T}_i = \mathbf{R}_i {}^i\mathbf{T}_j. \quad (3)$$

In this equation, the translation ${}^i\mathbf{T}_j$ is given by the structure of the robot, while all the others are variables to be determined through the IK process. Using this relation, we can write the translation of the end-effector as a function of the rotations along a path of links \mathcal{P}_{fk} . For $\forall i, j \in \mathcal{P}_{fk}$, we have

$$\begin{aligned} \mathbf{T}_{ee} &= \mathbf{T}_{base} + \sum_{i \in \mathcal{P}_{fk}} \mathbf{R}_i {}^i\mathbf{T}_j \\ &= \mathbf{T}_{base} + \sum_{i \in \mathcal{P}_{fk}} ({}^i\mathbf{T}_j^\top \otimes \mathbf{I}_3) \text{vec}(\mathbf{R}_i) \end{aligned} \quad (4)$$

We denote $\mathcal{P}_r \subset \mathcal{P}_{fk}$ including all the revolute and spherical joints and $\mathcal{P}_p \subset \mathcal{P}_{fk}$ including all the prismatic joints. If

there are only revolute or spherical joints along the path \mathcal{P}_{fk} (i.e., $\mathcal{P}_r = \mathcal{P}_{fk}$), equation (4) becomes a linear expression of end-effector location from the rotations. If there are prismatic joints within the path, then ${}^i\mathbf{T}_j$ is no longer a parameter and we will show that \mathbf{T}_{ee} can be written as a linear function of the rotations and an additional variable. These linear expressions allow us to algebraically eliminate the translations from our problem, and solve for the rotations alone (this is discussed more in detail in Section VII-A). Assuming the links are connected in a chain, and that at least one \mathbf{T}_i is known (e.g., the robot base is fixed), then all the translations can be recovered using (3) once the rotations and additional variables for prismatic joints are determined.

Remark 1: Observe that (4) enables us to impose additional structural constraints on the robot. For example, consider a situation where two manipulators are working collaboratively with their end-effectors rigidly attached. For each of them, the end-effector position is a function of its rotations \mathbf{R} . To fulfill the cooperation requirements we can simply let these two functions equal to each other, resulting in a linear constraint on the closed chain.

B. Revolute joint axis constraints

For each pair of links $(i, j) \in \mathcal{E}_r$ that are connected with a revolute joint, the orientations \mathbf{R}_i and \mathbf{R}_j are related by the equation

$$\mathbf{R}_j = \mathbf{R}_i \mathbf{R}_e \mathbf{R}_\theta \quad (5)$$

where $\mathbf{R}_\theta : \mathbb{R} \mapsto \mathbf{SO}(3)$ is a function of the joint angle θ (defined such that $\mathbf{R}_\theta = \mathbf{I}$ when $\theta = 0$), and \mathbf{R}_e is a parameter defined as the rotation from \mathcal{B}_j to \mathcal{B}_i when $\theta = 0$. Without loss of generality, we assume that \mathbf{R}_θ is a rotation about the z -axis, meaning that frames \mathcal{B}_i and \mathcal{B}_j share the same z -axis, that is:

$$\mathbf{R}_i \mathbf{R}_e \mathbf{e}_3 - \mathbf{R}_j \mathbf{e}_3 = \mathbf{0}. \quad (6)$$

Using the vectorization property of the Kronecker product, we have

$$(\mathbf{e}_3^\top \mathbf{R}_e^\top \otimes \mathbf{I}) \text{vec}(\mathbf{R}_i) - (\mathbf{e}_3^\top \otimes \mathbf{I}) \text{vec}(\mathbf{R}_j) = \mathbf{0}. \quad (7)$$

C. Revolute joint angle limits

In physical systems, the joint angle θ in (5) is limited to an interval $[-\phi_1, \phi_2]$. Without loss of generality, we can assume this interval to be symmetric, i.e., $\phi_1 = \phi_2 = \alpha$ (if not, we can translate the origin of the angle θ so that it is in the middle of the interval). With this assumption, the joint angle constraint becomes

$$|\theta| \leq \alpha. \quad (8)$$

We introduce a formulation of the angle limit constraints that is linear in the rotations and exactly captures (8), as shown in the following proposition.

Proposition 1: For a robot with links \mathcal{V} connected by relation \mathcal{E} and variables defined by (2), the revolute joint

angle limit constraint is satisfied if $\{\mathbf{R}_i\}$ are rotations, and for every $(\mathbf{R}_i, \mathbf{R}_j), (i, j) \in \mathcal{E}$, it holds that

$$\mathbf{R}_i \mathbf{R}_e \mathbf{e}_1 - \mathbf{R}_j \mathbf{e}_1 \in \mathcal{S}(\sqrt{2 - 2 \cos(\alpha_{ij})}), \quad (9)$$

where $\mathcal{S}(r)$ is a ball with radius r and centered at the origin.

Proof: Since the rotations \mathbf{R}_j and $\mathbf{R}_i \mathbf{R}_e$ in (5) share the same z -axis and their x - and y -axes are on the same plane. The angle θ can be seen as the angular displacement from the x -axis of $\mathbf{R}_i \mathbf{R}_e$ to that of \mathbf{R}_j . Therefore, for two vectors $\mathbf{w}_i = \mathbf{R}_i \mathbf{R}_e \mathbf{e}_1$ and $\mathbf{w}_j = \mathbf{R}_j \mathbf{e}_1$, we have $\theta = \angle(\mathbf{w}_i, \mathbf{w}_j)$ and (8) becomes $|\angle(\mathbf{w}_i, \mathbf{w}_j)| < \alpha_{ij}$. Substituting the axis constraint (5), and the expressions for $\mathbf{w}_i, \mathbf{w}_j$ into $\|\mathbf{w}_i - \mathbf{w}_j\|^2$ we have $\|\mathbf{w}_i - \mathbf{w}_j\|^2 = 2 - 2 \cos(\theta) \leq 2 - 2 \cos(\alpha_{ij})$ for $\theta \in [-\alpha_{ij}, \alpha_{ij}]$, which gives the bound in (9) (see Fig. 2 for a visualization). It is worth mentioning that (9) is algebraically equivalent to [4, Eq. (13)], but in different form. ■

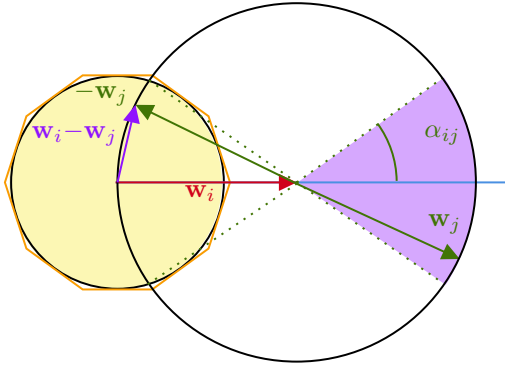


Fig. 2: The joint limit between two links $(i, j) \in \mathcal{E}_r$ can be written as an angle limit between two unit vectors $\mathbf{w}_i = \mathbf{R}_i \mathbf{R}_e \mathbf{e}_1$ and $\mathbf{w}_j = \mathbf{R}_j \mathbf{e}_1$ (purple sector), which can be further bounded by a ball (painted yellow) on $\mathbf{w}_i - \mathbf{w}_j$. The ball can be then approximated by linear inequalities (orange polygon).

D. Prismatic Joints

For two links (i, j) connected by a prismatic joint $(i, j) \in \mathcal{E}_p$, the physical limit of the joint restricts that 1) the orientation is preserved throughout the sliding of the links, and 2) the relative distance of the two links is bounded. A visualization of these relations is shown in Fig. 3, where the two links are sliding along a common axis with a bounded displacement. The orientation is preserved when $\mathbf{R}_i = \mathbf{R}_j$. Meanwhile (3) holds and can be written as

$$\mathbf{T}_j = \mathbf{T}_i + (\tau_l + \tau_i(\tau_u - \tau_l)) \mathbf{R}_i \mathbf{R}_p \mathbf{e}_3 \quad (10)$$

where \mathbf{R}_p is a parameter rotation and $\tau_i \in [0, 1]$ is a *bounded* variable that represents the extension of the joint, and τ_l, τ_u are the lower- and upper-limits of the joint extension. To simplify, we include $\mathbf{R}_i = \mathbf{R}_i \mathbf{R}_p$ as variables and drop the “ \sim ” notation. In this way, (10) becomes $\mathbf{T}_j = \mathbf{T}_i + (\tau_l + \tau_i(\tau_u - \tau_l)) \mathbf{R}_i \mathbf{e}_3$ and the actual \mathbf{R}_i can be recovered by multiplying \mathbf{R}_p^T . With this we give the following definition of prismatic joints.

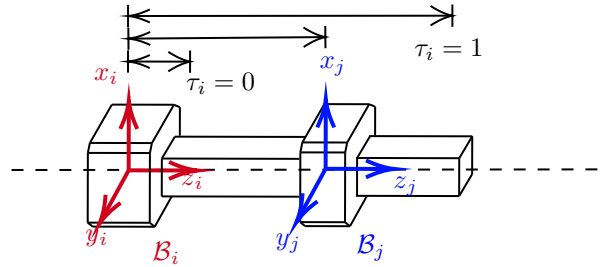


Fig. 3: Two links connected by a prismatic joint, where the two associated reference frames follow a bounded displacement along the common z -axis.

Definition 1: For a robot with links \mathcal{V} connected by relation \mathcal{E} and variables defined by (2), a prismatic joint $(i, j) \in \mathcal{E}_p$ is defined by the constraints:

$$\begin{aligned} \mathbf{R}_i &= \mathbf{R}_j, \\ \mathbf{R}_i, \mathbf{R}_j &\in \mathbf{SO}(3) \\ \mathbf{T}_j &= \mathbf{T}_i + (\tau_l + \tau_i(\tau_u - \tau_l)) \mathbf{R}_i^{(3)}, \\ \tau_i &\in [0, 1], \end{aligned} \quad (11)$$

where $\mathbf{R}_i^{(3)}$ is the third column of \mathbf{R}_i .

With (11), we can rewrite (4) as

$$\begin{aligned} \mathbf{T}_{ee} &= \mathbf{T}_{base} + \sum_{(i,j) \in \mathcal{P}_r} ({}^i \mathbf{T}_j^T \otimes \mathbf{I}_3) \text{vec}(\mathbf{R}_i) \\ &+ \sum_{(i,j) \in \mathcal{P}_p} (\tau_l + \tau_i(\tau_u - \tau_l)) \mathbf{R}_i^{(3)}. \end{aligned} \quad (12)$$

Equation (12) defines a linear mapping from the rotations to the translation of the end-effector, and by bounding the factor τ_i , we can restrict the relative distance of the links $(i, j) \in \mathcal{P}_p$.

VI. MODELING AND RELAXATION OF THE FEASIBLE SET

In this section we introduce how to model and relax the feasible set defined by the group of kinematic constraints. Our goal is to develop linear or semidefinite constraints.

A. Relaxation of the feasible set for revolute joints

Observe that the condition for joint axis in (7) is linear in the vectorized rotations. We therefore define

$$\mathbf{u} = \text{stack}(\{\text{vec}(\mathbf{R}_i)\}_{i \in \mathcal{V}_r}). \quad (13)$$

and concatenate (7) for each $(i, j) \in \mathcal{E}_r$, obtaining the constraint

$$\mathbf{A}_{\text{axis}} \mathbf{u} = \mathbf{b}_{\text{axis}}. \quad (14)$$

Next, from Proposition 1, the joint angle limit constraint requires that for every pair $(i, j) \in \mathcal{E}_r$, $(\mathbf{R}_i, \mathbf{R}_j)$ satisfies the ball bound (9), which can be approximated using linear inequalities, namely, a polyhedron. Specifically, for each $(i, j) \in \mathcal{E}_r$, we choose multiple points on the ball that bounds $\mathbf{w}_i - \mathbf{w}_j$ in (9), and the polyhedron is defined as the hull formed by all faces tangent to the ball at the selected points. Because \mathbf{w}_i and \mathbf{w}_j are linear in \mathbf{u} , the linear inequalities for all $(i, j) \in \mathcal{E}_r$ can then be concatenated as

$$\mathbf{A}_{\text{angle}} \mathbf{u} \leq \mathbf{b}_{\text{angle}}. \quad (15)$$

B. Relaxation of $\mathbf{SO}(3)$

The definition of \mathbf{u} requires that each $\mathbf{R}_i \in \mathbf{SO}(3)$, i.e.,

$$\mathbf{R}_i^\top \mathbf{R}_i = \mathbf{I}_3 \text{ and } \det(\mathbf{R}_i) = +1. \quad (16)$$

These constraints are nonconvex in \mathbf{u} . We propose a novel way to relax $\mathbf{SO}(3)$ using convex constraints. For $\mathbf{R}_i = \begin{bmatrix} \mathbf{R}_i^{(1)} & \mathbf{R}_i^{(2)} & \mathbf{R}_i^{(3)} \end{bmatrix}$, equation (16) is equivalent to

$$\begin{aligned} \|\mathbf{R}_i^{(1)}\| &= 1 \\ \|\mathbf{R}_i^{(2)}\| &= 1 \\ \mathbf{R}_i^{(1)} \cdot \mathbf{R}_i^{(2)} &= 0 \\ \mathbf{R}_i^{(1)} \times \mathbf{R}_i^{(2)} &= \mathbf{R}_i^{(3)} \end{aligned} \quad (17)$$

For every rotation $\mathbf{R}_i, i \in \mathcal{V}_r$, we define a new variable

$$\mathbf{Y}_i = \begin{bmatrix} \mathbf{R}_i^{(1)} \\ \mathbf{R}_i^{(2)} \\ 1 \end{bmatrix} \begin{bmatrix} \mathbf{R}_i^{(1)} \\ \mathbf{R}_i^{(2)} \\ 1 \end{bmatrix}^\top \in \mathbb{R}^{7 \times 7}. \quad (18)$$

Observe that \mathbf{Y}_i is a symmetric rank-1 matrix with the top left 6×6 block containing all the element-wise multiplication of $(\mathbf{R}_i^{(1)}, \mathbf{R}_i^{(1)}), (\mathbf{R}_i^{(1)}, \mathbf{R}_i^{(2)})$, and $(\mathbf{R}_i^{(2)}, \mathbf{R}_i^{(2)})$. The last column of \mathbf{Y}_i consists of $\mathbf{R}_i^{(1)}, \mathbf{R}_i^{(2)}$, and 1. The advantages of choosing this structure are that:

- 1) the first three equations of (17) are linear in \mathbf{Y}_i and can be concatenated in a single linear equality constraint;
- 2) $\mathbf{R}_i^{(1)} \times \mathbf{R}_i^{(2)}$ is linear in \mathbf{Y}_i , meaning that we can represent $\mathbf{R}_i^{(3)}$ as a linear function of \mathbf{Y}_i ;
- 3) since each column of \mathbf{R}_i is linear in \mathbf{Y}_i , there exists a linear transformation g such that $\mathbf{u} = g(\mathbf{Y})$, $\mathbf{Y} = \{\mathbf{Y}_i\}_{i \in \mathcal{V}_r}$, which makes the revolute joint axis and angle limit constraints linear in \mathbf{Y}_i as well.

Definition 2: We define explicitly the linear transformation $g(\mathbf{Y}) : \mathbb{R}^{7 \times 7 n_r} \mapsto \mathbb{R}^{9 n_r}$ which is given by the composition of the following operations.

- 1) For each \mathbf{Y}_i , extract the first and second 3×1 vectors of the last column \mathbf{y}_{1i} and \mathbf{y}_{2i} .
- 2) Compute $\mathbf{y}_{3i} = \mathbf{y}_{1i} \times \mathbf{y}_{2i}$ using the needed elements from the top left 6×6 block of \mathbf{Y}_i . Explicitly,

$$\mathbf{y}_{3i} = \begin{bmatrix} \mathbf{Y}_i(2, 6) - \mathbf{Y}_i(3, 5) \\ \mathbf{Y}_i(3, 4) - \mathbf{Y}_i(1, 6) \\ \mathbf{Y}_i(1, 5) - \mathbf{Y}_i(2, 4) \end{bmatrix}. \quad (19)$$

- 3) Concatenate vertically $\mathbf{y}_{1i}, \mathbf{y}_{2i}$, and \mathbf{y}_{3i} in sequence for all $i \in \mathcal{V}_r$.

Definition 3: In order to enforce the relations in (17) and the structure defined in (18), we define the constraint

$$\mathbf{A}_{\text{structure}} \text{vec}(\mathbf{Y}) = \mathbf{b}_{\text{structure}} \quad (20)$$

that imposes the following structure on \mathbf{Y} : for each \mathbf{Y}_i ,

- 1) $\text{tr}(\mathbf{Y}_i(1 : 3, 1 : 3)) = \text{tr}(\mathbf{Y}_i(4 : 6, 4 : 6)) = 1$;
- 2) $\text{tr}(\mathbf{Y}_i(1 : 3, 4 : 6)) = 0$;
- 3) $\mathbf{Y}_i(7, 7) = 1$.

Our proposed relaxation of $\mathbf{SO}(3)$ is obtained by developing the rank-1 constraint in the following proposition.

Proposition 2: A real 3×3 matrix $\hat{\mathbf{R}}$ is on the set $\mathbf{SO}(3)$ if and only if $\text{vec}(\hat{\mathbf{R}}) = g(\hat{\mathbf{Y}})$, where $\hat{\mathbf{Y}} \in \mathbb{S}_+^7$ satisfies (20) and $\text{rank}(\hat{\mathbf{Y}}) = 1$.

Proof: For any $\hat{\mathbf{Y}}$ that satisfies $\hat{\mathbf{Y}} \succeq 0$ and $\text{rank}(\hat{\mathbf{Y}}) = 1$, we can write $\hat{\mathbf{Y}}$ as

$$\hat{\mathbf{Y}} = \begin{bmatrix} \mathbf{y}_1 \\ \mathbf{y}_2 \\ 1 \end{bmatrix} \begin{bmatrix} \mathbf{y}_1 \\ \mathbf{y}_2 \\ 1 \end{bmatrix}^\top, \quad \mathbf{y}_1, \mathbf{y}_2 \in \mathbb{R}^3. \quad (21)$$

The structural constraint (20) acts on the entries of $\hat{\mathbf{Y}}$ such that

$$\begin{cases} \text{tr}(\mathbf{y}_1 \mathbf{y}_1^\top) = \text{tr}(\mathbf{y}_2 \mathbf{y}_2^\top) = 1 \\ \text{tr}(\mathbf{y}_1 \mathbf{y}_2^\top) = 0 \end{cases} \quad (22)$$

which is equivalent to $\|\mathbf{y}_1\| = \|\mathbf{y}_2\| = 1$ and $\mathbf{y}_1^\top \mathbf{y}_2 = 0$. We form a new matrix $\tilde{\mathbf{R}} = \begin{bmatrix} \mathbf{y}_1 & \mathbf{y}_2 & \mathbf{y}_1 \times \mathbf{y}_2 \end{bmatrix}$. When $\text{rank}(\hat{\mathbf{Y}}) = 1$, the linear operation in step 2 of Definition 2 recovers $\mathbf{y}_1 \times \mathbf{y}_2$ exactly and therefore $\tilde{\mathbf{R}} = \hat{\mathbf{R}}$. It is clear that $\tilde{\mathbf{R}}$ satisfies (17) and thus (16) and $\hat{\mathbf{R}} = \tilde{\mathbf{R}} \in \mathbf{SO}(3)$.

On the other hand, for any $\hat{\mathbf{R}} \in \mathbf{SO}(3)$, we can always use (18) to construct a corresponding rank-1 $\hat{\mathbf{Y}}$ that satisfies (20), $\hat{\mathbf{Y}} \succeq 0$, and $\text{rank}(\hat{\mathbf{Y}}) = 1$. \blacksquare

C. Relaxation of prismatic joints

The constraint (11) for a prismatic joint involves a bi-linear term $\tau_i \mathbf{R}_i^{(3)}$. To be able to include this constraint in the SDP problem, for each prismatic joint $(i, j) \in \mathcal{E}_p$, we introduce a new decision variable

$$\mathbf{Y}_{\tau i} = \begin{bmatrix} \sqrt{\tau_i} \mathbf{R}_i^{(3)} \\ \sqrt{1 - \tau_i} \mathbf{R}_i^{(3)} \\ \frac{\sqrt{\tau_i}}{\sqrt{1 - \tau_i}} \end{bmatrix} \begin{bmatrix} \sqrt{\tau_i} \mathbf{R}_i^{(3)} \\ \sqrt{1 - \tau_i} \mathbf{R}_i^{(3)} \\ \frac{\sqrt{\tau_i}}{\sqrt{1 - \tau_i}} \end{bmatrix}^\top \in \mathbb{R}^{8 \times 8}, \quad (23)$$

The prismatic constraint (11) is linear in $\mathbf{Y}_{\tau i}$.

Remark 2: To include (11), we do not need the entire $\mathbf{Y}_{\tau i}$. The additional entries are to give the property that $\text{tr}(\mathbf{Y}_{\tau i})$ is a constant, which is important for the rank minimization process introduced in Section VII.

We define constraints

$$\begin{aligned} \mathbf{A}_{p0,eq} \text{vec}(\mathbf{Y}_\tau) &= \mathbf{b}_{p0,eq} \\ \mathbf{A}_{p,ieq} \text{vec}(\mathbf{Y}_\tau) &\leq \mathbf{b}_{p,ieq} \\ \mathbf{A}_{p1,eq} \text{vec}(\mathbf{Y}) + \mathbf{A}_{p2,eq} \text{vec}(\mathbf{Y}_\tau) &= \mathbf{b}_{p1,eq} \end{aligned} \quad (24)$$

to restrict the following linear relations of $\mathbf{Y}_{\tau i}$ and \mathbf{Y}_i entries: for $(i, j) \in \mathcal{E}_p$,

- 1) the trace of $\mathbf{Y}_{\tau i}$ equals 2;
- 2) $\text{tr}(\mathbf{Y}_{\tau i}(1 : 3, 1 : 3)) = \mathbf{Y}_{i\tau}(7, 7)$ and $\text{tr}(\mathbf{Y}_{\tau i}(4 : 6, 4 : 6)) = \mathbf{Y}_{i\tau}(8, 8)$;
- 3) $\mathbf{Y}_{\tau i}(4 : 6, 7) = \mathbf{Y}_{\tau i}(1 : 3, 8)$;
- 4) $\text{tr}(\mathbf{Y}_{\tau i}(1 : 3, 4 : 6)) = \mathbf{Y}_{\tau i}(7, 8)$;
- 5) $\mathbf{Y}_{\tau i}(7, 7) \in [0, 1]$;
- 6) $\mathbf{Y}_{\tau i}(7, 8) \geq 0$;
- 7) $\mathbf{Y}_{\tau i}(1 : 3, 7) + \mathbf{Y}_{\tau i}(4 : 6, 8) = \text{r.h.s. of (19)}$.

The relations 1)-4) describes the equality of parts in \mathbf{Y}_{τ_i} when $\|\mathbf{R}^{(3)}\| = 1$, including

$$\begin{aligned} \|\sqrt{\tau_i}\mathbf{R}_i^{(3)}\|_2^2 + \|\sqrt{1-\tau_i}\mathbf{R}_i^{(3)}\|_2^2 + \|\sqrt{\tau_i}\|_2^2 + \|\sqrt{1-\tau_i}\|_2^2 &= 2 \\ \|\sqrt{\tau_i}\mathbf{R}_i^{(3)}\|_2^2 &= \|\sqrt{\tau_i}\|_2^2 \\ \|\sqrt{1-\tau_i}\mathbf{R}_i^{(3)}\|_2^2 &= \|\sqrt{1-\tau_i}\|_2^2 \\ \sqrt{1-\tau_i}\mathbf{R}_i^{(3)} \cdot \sqrt{\tau_i} &= \sqrt{\tau_i}\mathbf{R}_i^{(3)} \cdot \sqrt{1-\tau_i} \\ \sqrt{\tau_i(1-\tau_i)} \operatorname{tr}(\mathbf{R}_i^{(3)}\mathbf{R}_i^{(3)\top}) &= \sqrt{\tau_i(1-\tau_i)} \end{aligned} \quad (25)$$

The constraint 5) enforces that $\tau_i \in [0, 1]$.

Constraint 6) is to make sure that the part $\mathbf{Y}_{\tau_i}(1:3, 4:6)$ is restricted by a constraint such that the SDP solver does not assign all-zeros to these entries. In fact, 6) is useful in the proof of Proposition 3 below.

Constraint 7) is a linear constraint on \mathbf{Y}_{τ_i} and \mathbf{Y}_i where the left hand side is an analogue of $\tau_i\mathbf{R}_i^{(3)} + (1-\tau_i)\mathbf{R}_i^{(3)}$ while the right hand side is a linear function of \mathbf{Y}_i as discussed in Definition 2. This constraint is to yield that the $\mathbf{R}_i^{(3)}$ extracted from \mathbf{Y}_{τ_i} is exactly $\mathbf{R}_i^{(1)} \times \mathbf{R}_i^{(2)}$ from \mathbf{Y}_i .

Proposition 3: Equations (11) hold if and only if

$$\mathbf{T}_j = \mathbf{T}_i + \tau_l\mathbf{R}_i^{(3)} + (\tau_u - \tau_l)\mathbf{Y}_{\tau_i}(1:3, 7), \quad (26)$$

$\mathbf{Y}_i, \mathbf{Y}_{\tau_i} \in \mathbb{S}_+$ satisfy (24), \mathbf{Y}_i satisfies (20), $\mathbf{R}_i = \mathbf{R}_j$, and $\operatorname{rank}(\mathbf{Y}_i) = \operatorname{rank}(\mathbf{Y}_{\tau_i}) = 1$.

Proof: For the “if” part, any rank-1 \mathbf{Y}_{τ_i} satisfying (24) can be written as

$$\mathbf{Y}_{\tau_i} = \begin{bmatrix} \sqrt{t}\mathbf{y}_1 \\ \sqrt{(1-t)}\mathbf{y}_1 \\ \pm\sqrt{t} \\ \pm\sqrt{1-t} \end{bmatrix} \begin{bmatrix} \sqrt{t}\mathbf{y}_1 \\ \sqrt{(1-t)}\mathbf{y}_1 \\ \pm\sqrt{t} \\ \pm\sqrt{1-t} \end{bmatrix}^\top, \quad (27)$$

where $\operatorname{tr}(\mathbf{y}_1\mathbf{y}_1^\top) = 1$, $t \in [0, 1]$ and the “ \pm ” in the last two entries of the multiplier vector take the same sign. A separate proof of this claim is provided in the appendix. When $\operatorname{rank}(\mathbf{Y}_i) = 1$ and the sign is “+”, by 7) in (24) and Proposition 2 we have $t\mathbf{y}_1 + (1-t)\mathbf{y}_1 = \mathbf{y}_1 = \mathbf{R}_i^{(3)}$. On the other hand, when the sign is “-”, similarly we have $-t\mathbf{y}_1 + (1-t)\mathbf{y}_1 = -\mathbf{y}_1 = \mathbf{R}_i^{(3)}$. Therefore $\mathbf{Y}_{\tau_i}(1:3, 7) = \pm t\mathbf{y}_1 = t\mathbf{R}_i^{(3)}$ and (26) becomes (11). For the “only if” part, given rotation \mathbf{R}_i , translation \mathbf{T}_i and scalar τ_i that satisfy (11), we can use (23) to construct a rank-1 $\mathbf{Y}_{\tau_i} \succeq 0$ that satisfies (24). And by Proposition 2 we have $\mathbf{Y}_i \succeq 0$ satisfies (20) and $\operatorname{rank}(\mathbf{Y}_i) = 1$. ■

D. Relaxation of the feasible set and its properties

Because our kinematic constraints involve solving for rotation matrices of the reference frames attached to the free parents of revolute joints and pairs of links connected by prismatic joints, the set \mathcal{V}_r is the set of vertices for these frames. For convenience, we denote the set of vertices associated with the parents of the prismatic joints as $\mathcal{V}_p := \{i|(i, j) \in \mathcal{E}_p\}$. We define below the original and relaxed feasible sets.

Definition 4: We define \mathcal{U} as the set of the vectors $\mathbf{u} = \operatorname{stack}(\{\operatorname{vec}(\mathbf{R}_i)|i \in \mathcal{V}_r\})$ and $\boldsymbol{\tau} := \{\tau_i|i \in \mathcal{V}_p\}$ such that

$$\mathbf{A}_{\text{axis}}\mathbf{u} = \mathbf{b}_{\text{axis}}, \quad (28a)$$

$$\mathbf{A}_{\text{angle}}\mathbf{u} \leq \mathbf{b}_{\text{angle}}, \quad (28b)$$

$$\mathbf{A}_{\text{parallel}}\mathbf{u} = \mathbf{b}_{\text{parallel}}, \quad (28c)$$

$$\mathbf{R}_i \in \mathbf{SO}(3), \forall i \in \mathcal{V}_r \quad (28d)$$

$$\tau_i \in [0, 1], i \in \mathcal{V}_p. \quad (28e)$$

The equality (28c) is a constraint on $(i, j) \in \mathcal{E}_p$ such that $\mathbf{R}_i = \mathbf{R}_j$. We define also the set \mathcal{Y} of

$$\begin{aligned} \mathbf{Y} &:= \{\mathbf{Y}_i|\mathbf{Y}_i = y(\mathbf{u})\}_{i \in \mathcal{V}_r} \text{ and} \\ \mathbf{Y}_\tau &:= \{\mathbf{Y}_{\tau_i}|\mathbf{Y}_{\tau_i} = y_\tau(\mathbf{u}, \boldsymbol{\tau})\}_{i \in \mathcal{V}_p}, \end{aligned} \quad (29)$$

where y and y_τ are functions of \mathbf{u} and $\boldsymbol{\tau}$ defined in (18) and (23), respectively. We then define the relaxed set $\bar{\mathcal{Y}} := \{\bar{\mathbf{Y}}_i\}_{i \in \mathcal{V}_r}$ and $\bar{\mathbf{Y}}_\tau := \{\bar{\mathbf{Y}}_{\tau_i}\}_{i \in \mathcal{V}_p}$ such that

$$\bar{\mathbf{Y}} = \{\bar{\mathbf{Y}}_i \in \mathbb{S}_+^7|i \in \mathcal{V}_r\}, \quad (30a)$$

$$\bar{\mathbf{Y}}_\tau = \{\bar{\mathbf{Y}}_{\tau_i} \in \mathbb{S}_+^8|i \in \mathcal{V}_p\}, \quad (30b)$$

$$\mathbf{A}_{\text{axis}}g(\bar{\mathbf{Y}}) = \mathbf{b}_{\text{axis}}, \quad (30c)$$

$$\mathbf{A}_{\text{angle}}g(\bar{\mathbf{Y}}) \leq \mathbf{b}_{\text{angle}}, \quad (30d)$$

$$\mathbf{A}_{\text{parallel}}g(\bar{\mathbf{Y}}) = \mathbf{b}_{\text{parallel}}, \quad (30e)$$

$$\mathbf{A}_{\text{structure}}\operatorname{vec}(\bar{\mathbf{Y}}) = \mathbf{b}_{\text{structure}}, \quad (30f)$$

$$\bar{\mathbf{Y}}, \bar{\mathbf{Y}}_\tau \text{ satisfy (24)}. \quad (30g)$$

For convenience, $\bar{\mathcal{U}}$ refers to the set of the image of $\bar{\mathcal{Y}}$ through transformation g and the extraction of $\boldsymbol{\tau}$ from \mathbf{Y}_τ , i.e., $\bar{\mathcal{U}} := \operatorname{image}(\bar{\mathcal{Y}}) = \{g(\bar{\mathbf{Y}}), \{\bar{\mathbf{Y}}_{\tau_i}(7, 7)\}_{i \in \mathcal{V}_p}|\bar{\mathbf{Y}}, \bar{\mathbf{Y}}_\tau \in \bar{\mathcal{Y}}\}$. The set \mathcal{R}_1 refers to the set of rank-1 matrices: $\mathcal{R}_1 := \{\mathbf{Y}, \mathbf{Y}_\tau|\operatorname{rank}(\mathbf{Y}_i) = \operatorname{rank}(\mathbf{Y}_{\tau_j}) = 1, \forall i \in \mathcal{V}_r, j \in \mathcal{V}_p\}$.

We show some useful results about \mathcal{U} and \mathcal{Y} .

Proposition 4: The set $\bar{\mathcal{Y}}$ is bounded.

Proof: Any $\mathbf{Y}_i \succeq 0$ can be decomposed as $\mathbf{Y}_i = U\Sigma U^\top$ where U is an orthonormal matrix and Σ is a diagonal matrix containing all the eigenvalues of \mathbf{Y}_i . The set \mathcal{Y} defined in (30) is bounded because every element of U belongs to $[0, 1]$, while (30f) and (30a) restrict each elements of Σ to the interval $[0, 3]$. Every \mathbf{Y}_{τ_i} can be also decomposed into matrices that are bounded by the constraints in (24). ■

Proposition 5: The set $\bar{\mathcal{U}}$ contains every element of \mathcal{U} , i.e., $\mathcal{U} \subset \bar{\mathcal{U}}$.

Proof: This is a consequence of the fact that we can build $\mathbf{Y}, \mathbf{Y}_\tau \in \mathcal{Y}$ that satisfy all the constraints of $\bar{\mathcal{Y}}$ for any $\mathbf{u} \in \mathcal{U}$ using (18) and (23). ■

Proposition 6: The set $\bar{\mathcal{U}}$ exactly matches the set \mathcal{U} if $\bar{\mathcal{U}} = \operatorname{image}(\bar{\mathcal{Y}} \cap \mathcal{R}_1) = \{g(\bar{\mathbf{Y}}), \{\bar{\mathbf{Y}}_{\tau_i}(7, 7)\}_{i \in \mathcal{V}_p}|\bar{\mathbf{Y}}, \bar{\mathbf{Y}}_\tau \in \bar{\mathcal{Y}} \cap \mathcal{R}_1\}$.

Proof: Using Proposition 2 we know that for any $\mathbf{u} = \operatorname{stack}(\{\operatorname{vec}(\mathbf{R}_i)|i \in \mathcal{V}_r\}) \in \mathcal{U}$, we have $\mathbf{R}_i \in \mathbf{SO}(3), \forall i \in \mathcal{V}_r$ if and only if every corresponding \mathbf{Y}_i as a function of \mathbf{R}_i through (18) satisfies (30f), $\mathbf{Y}_i \succeq 0$, and $\operatorname{rank}(\mathbf{Y}_i) = 1$. Therefore the equivalence hold between (28d) and $\{(30a), (30b), (30f)\} \cap \mathcal{R}_1$. According to Proposition 3, for every $(i, j) \in \mathcal{E}_p$, $\mathbf{R}_i = \mathbf{R}_j \in \mathbf{SO}(3)$, $\tau_i \in [0, 1]$ hold if and only if $\mathbf{Y}, \mathbf{Y}_\tau$ satisfy (24) (enforced by (30g)), $\mathbf{R}_i = \mathbf{R}_j$

(enforced by (30e)), and $\text{rank}(\mathbf{Y}_{\tau_i}) = 1$. The equivalence hold between the constraints on revolute joints, i.e., $\{(28a), (28b)\}$ and $\{(30c), (30d)\} \cap \mathcal{R}_1$ and all the constraints in $\bar{\mathcal{Y}}$ and $\bar{\mathcal{U}}$ are covered. ■

Proposition 7: The set \mathcal{U} is a subset of the boundary of $\bar{\mathcal{U}}$, i.e., $\mathcal{U} \subset \partial\bar{\mathcal{U}}$.

Proof: From Proposition 6 we have $\mathcal{U} = \bar{\mathcal{U}}$ if $\bar{\mathcal{U}} = \text{image}(\bar{\mathcal{Y}} \cap \mathcal{R}_1)$. Thus for any $\mathbf{u} = g(\mathbf{Y}) \in \mathcal{U}$, each \mathbf{Y}_i of \mathbf{Y} is rank-1 and has a zero eigenvalue. Therefore, there exists a matrix \mathbf{M} such that $\tilde{y}_i(t) = \mathbf{Y}_i + t\mathbf{M} \notin \mathbb{S}_+$ and $\tilde{\mathbf{u}} = g(\tilde{y}(t)) \notin \bar{\mathcal{U}}$ for any $t > 0$. Thus $\mathbf{u} = g(\mathbf{Y})$ is on the boundary of $\bar{\mathcal{U}}$. ■

VII. OPTIMIZATION

This section first introduces how to build an inverse kinematics optimization problem, then discusses how to relax this problem using the relaxed set defined in Section VI, and finally introduces a rank minimization algorithm to find low-rank solutions, with local convergence guarantees toward the exact solutions of the original IK problem.

A. Inverse kinematics problem

The inverse kinematics problem aims to find the optimal and feasible \mathbf{x}^* such that the end-effector ee , reaches a desired location \mathbf{T}_{goal} and orientation \mathbf{R}_{goal} . This objective can be encoded as

$$\|\text{vec}(\mathbf{R}_{ee}) - \text{vec}(\mathbf{R}_{goal})\|_2^2 + \|\mathbf{T}_{ee} - \mathbf{T}_{goal}\|_2^2. \quad (31)$$

We define a selection matrix $\mathbf{E}_{ee} \in \mathbb{R}^{3n \times 3}$ such that $\mathbf{R}\mathbf{E}_{ee} = \mathbf{R}_{ee}$ then substitute it along with (12) into the cost to get

$$\begin{aligned} f_0(\mathbf{R}, \{\tau_i\}) = & \|(\mathbf{E}_{ee}^\top \otimes \mathbf{I}_3)\text{vec}(\mathbf{R}) - \text{vec}(\mathbf{R}_{goal})\|_2^2 \\ & + \|\mathbf{T}_{base} + \sum_{(i,j) \in \mathcal{P}_r} ({}^i\mathbf{T}_j^\top \otimes \mathbf{I}_3)\text{vec}(\mathbf{R}_i) \\ & + \sum_{(i,j) \in \mathcal{P}_p} (\tau_l + \tau_i(\tau_u - \tau_l))\mathbf{R}_i^{(3)} - \mathbf{T}_{goal}\|_2^2 \end{aligned} \quad (32)$$

Vectorizing (32) and using Proposition 3, we can define an equivalent quadratic function $f(\mathbf{Y}, \mathbf{Y}_\tau)$ such that $f(\mathbf{Y}, \mathbf{Y}_\tau) = f_0(\mathbf{R}, \{\tau_i\})$, where $\mathbf{Y}, \mathbf{Y}_\tau$ are constructed from $\mathbf{R}, \{\tau_i\}$. Our inverse kinematics problem is then defined as

Problem 1 (Inverse kinematics):

$$\min_{\mathbf{Y}, \mathbf{Y}_\tau} f(\mathbf{Y}, \mathbf{Y}_\tau) \quad (33a)$$

$$\text{subject to} \quad \mathbf{Y}, \mathbf{Y}_\tau \in \mathcal{Y} \quad (33b)$$

As defined above, \mathcal{Y} is the exact feasible set of the kinematic constraints. When $f(\mathbf{Y}, \mathbf{Y}_\tau) = 0$, from (31) we know that the pose of the end-effector matches the target.

B. Rank constrained problem and relaxations

Using Proposition 6 we can equivalently write the inverse kinematics problem as

Problem 2a (Rank constrained inverse kinematics):

$$\min_{\mathbf{Y}, \mathbf{Y}_\tau} f(\mathbf{Y}, \mathbf{Y}_\tau) \quad (34a)$$

$$\text{subject to} \quad \mathbf{Y}, \mathbf{Y}_\tau \in \bar{\mathcal{Y}} \quad (34b)$$

$$\text{rank}(\mathbf{Y}_i) = 1, \quad i \in \mathcal{V}_r \quad (34c)$$

$$\text{rank}(\mathbf{Y}_{\tau_i}) = 1, \quad i \in \mathcal{V}_p \quad (34d)$$

This problem has a quadratic objective function and convex constraints except for (34c) and (34d). We define the following relaxed problem which is obtained from Problem 2a with the omission of the rank constraints.

Problem 2b (Relaxed inverse kinematics):

$$\min_{\mathbf{Y}, \mathbf{Y}_\tau} f(\mathbf{Y}, \mathbf{Y}_\tau) \quad (35a)$$

$$\text{subject to} \quad \mathbf{Y}, \mathbf{Y}_\tau \in \bar{\mathcal{Y}} \quad (35b)$$

Remark 3: If Problem 2b is an infeasible problem, then Problem 2a is also infeasible, and if a solution $\mathbf{Y}^*, \mathbf{Y}_\tau^*$ is optimal for Problem 2b and $\mathbf{Y}^*, \mathbf{Y}_\tau^* \in \mathcal{Y}$, then it is also optimal for Problem 2a.

Remark 3 provides us a way to certify the infeasibility of the IK problem. If there exists no feasible problem when trying to solve Problem 2b, we are certain that there exists no feasible solution in the original feasible set \mathcal{U} .

C. Rank minimization via eigenvalue maximization

We propose two ways to solve for rank-1 matrices by manipulating their eigenvalues. The first can result in faster convergence but only works under an assumption. The second is slower in practice while requires no assumption. We introduce the first method in this section.

Proposition 8: Consider PSD matrices $\mathbf{M} \in \mathbb{S}_+^m$, with eigenvalues $\lambda_1 \geq \dots \geq \lambda_m$. Consider the function $\lambda_1(\mathbf{M}) = \lambda_1$ subject to the constraint $\text{tr}(\mathbf{M}) = c$ and $c > 0$, \mathbf{M}_0 is a rank-1 matrix if and only if $\mathbf{M}_0 = \text{argmax}(\lambda_1(\mathbf{M}))$.

Proof: The trace of a matrix is also the sum of all of its eigenvalues, which are all non-negative when the matrix is positive semidefinite. For the “if” direction, when the constant $\text{tr}(\mathbf{M}) = c$, we have $\lambda_i \leq c$, and the condition $\mathbf{M}_0 = \text{argmax}(\lambda_1(\mathbf{M}))$ is achieved when $\lambda_1(\mathbf{M}_0) = c$, implying $\lambda_2(\mathbf{M}_0), \dots, \lambda_m(\mathbf{M}_0) = 0$, and hence $\text{rank}(\mathbf{M}_0) = 1$. For the “only if” direction, under the constant $\text{tr}(\mathbf{M}) = c$, $\text{rank}(\mathbf{M}_0) = 1$ implies that the only positive eigenvalue $\lambda_1(\mathbf{M}_0)$ equals c , and since $0 \leq \lambda_i(\mathbf{M}) \leq c$ we have $\mathbf{M}_0 = \text{argmax}(\lambda_1(\mathbf{M}))$. ■

Assumption 1: Problem 1 is feasible and the optimal solution $\{\mathbf{Y}^*, \mathbf{Y}_\tau^*\} = \text{argmin}(f(\mathbf{Y}, \mathbf{Y}_\tau))$ lies within the feasible set $\bar{\mathcal{Y}}$.

Observe that the structure constraints (30f) and (30g) in (33b) of Problem 2a restrict that the trace of each \mathbf{Y}_i always equals 3 and the trace of each \mathbf{Y}_{τ_i} always equals 2. Under Assumption 1 and using Proposition 8 we can rewrite Problem 2a as the following problem:

Problem 2c (Eigenvalue maximization):

$$\max_{\mathbf{Y}, \mathbf{Y}_\tau} \sum_{i \in \mathcal{V}_r} \lambda_1(\mathbf{Y}_i) + \sum_{j \in \mathcal{V}_p} \lambda_1(\mathbf{Y}_{\tau j}) \quad (36a)$$

$$\text{subject to } \{\mathbf{Y}, \mathbf{Y}_\tau\} = \text{argmin}(f(\mathbf{Y}, \mathbf{Y}_\tau)) \quad (36b)$$

$$\mathbf{Y}, \mathbf{Y}_\tau \in \bar{\mathcal{Y}} \quad (36c)$$

$$(36d)$$

Notice that it is assumed in the above problem that the optimal solution exists in relaxed set, meaning that there exists an end-effector pose that reaches the desired pose. The rank minimization algorithm in this section only considers this situation, while an alternative approach that can minimize ranks without such assumption is discussed in VII-D.

We propose a gradient-based approach to Problem 2c. The idea is to increase the largest eigenvalue and the other eigenvalues will decrease because the traces of our variables are fixed. To begin with, we define the following operator to simplify the formulation.

$$Z(\mathbf{A}, \mathbf{v}) = \text{vec}(\mathbf{A})^\top (\mathbf{v} \otimes \mathbf{v}) \quad (37)$$

To find solution for Problem 2c we first find a solution to Problem 2b and then minimize the rank iteratively. In each step, the following problem is solved.

Problem 3 (Update):

$$\max_{\mathbf{U}^k, \mathbf{U}_\tau^k} \sum_{i \in \mathcal{V}_r} Z(\mathbf{U}_i^k, \mathbf{v}_i^{k-1, (1)}) + \sum_{j \in \mathcal{V}_p} Z(\mathbf{U}_{\tau j}^k, \mathbf{v}_{\tau j}^{k-1, (1)}) \quad (38a)$$

$$\text{subject to } \nabla f(\mathbf{Y}^{k-1} + \mathbf{U}^k, \mathbf{Y}_\tau^{k-1} + \mathbf{U}_\tau^k) = \mathbf{0} \quad (38b)$$

$$\mathbf{Y}^{k-1} + \mathbf{U}^k, \mathbf{Y}_\tau^{k-1} + \mathbf{U}_\tau^k \in \bar{\mathcal{Y}}_\tau \quad (38c)$$

The variable \mathbf{U}^k is an update of \mathbf{Y}^k , i.e., $\mathbf{Y}_i^k = \mathbf{Y}_i^{k-1} + \mathbf{U}_i^k$ and likely \mathbf{U}_τ^k is an update of \mathbf{Y}_τ^k . The objective function (38a) is the sum of inner products of the update and the gradient of the largest eigenvalues. For example, $Z(\mathbf{U}_i^k, \mathbf{v}_i^{k-1, (1)})$ is the inner product of $\text{vec}(\mathbf{U}_i^k)$ and the gradient of the largest eigenvalue λ_1 of \mathbf{Y}_i^{k-1} with respect to \mathbf{Y}_i^{k-1} itself, which can be computed using Lemma 1:

$$\begin{aligned} & \sum_{i \in \mathcal{V}_r} \text{vec}(\mathbf{U}_i^k)^\top \frac{\partial \lambda_1(\mathbf{Y}_i^{k-1})}{\partial \mathbf{Y}_i^{k-1}} \\ &= \sum_{i \in \mathcal{V}_r} \text{vec}(\mathbf{U}_i^k)^\top (\mathbf{v}_i^{k-1, (1)} \otimes \mathbf{v}_i^{k-1, (1)}), \end{aligned} \quad (39)$$

where $\mathbf{v}_i^{k-1, (1)}$ is the normalized eigenvector of \mathbf{Y}_i^{k-1} corresponding to λ_1 . Together, (38a) ensures that each \mathbf{U}_i^k and $\mathbf{U}_{\tau j}^k$ moves in the direction of the largest possible improvement in terms of increasing the sum of largest eigenvalues of \mathbf{Y}_i^k and $\mathbf{Y}_{\tau k, j}$, respectively. Since the traces of these two matrices are both fixed, when the largest eigenvalues are increased, the other eigenvalues will decrease and move \mathbf{Y}_i^k and $\mathbf{Y}_{\tau k}^k$ toward a rank-1 matrix. The constraint (38b) is the linear function of \mathbf{Y}^k and \mathbf{Y}_τ^k derived by differentiating the quadratic f with respect to \mathbf{Y} and \mathbf{Y}_τ and letting it equal to zeros, which ensures that $f(\mathbf{Y}^k, \mathbf{Y}_\tau^k) = f(\mathbf{Y}^0, \mathbf{Y}_\tau^0) = 0$ throughout the iterations, where \mathbf{Y}^0 and \mathbf{Y}_τ^0 are the solution of Problem 2b. The constraint (38c) makes sure that the updated \mathbf{Y}^k and \mathbf{Y}_τ^k remain on the feasible set $\bar{\mathcal{Y}}_\tau$.

D. An alternative approach for rank minimization

The rank minimization process in the previous section only works when Assumption 1 holds. In practice there exists IK problems where we don't know if there are feasible solutions that result in the optimal cost of the relaxed problem. For example, sometimes we want to find the joint configurations that lead the end-effector to be *as close as possible* to a target that is too far for the robot to reach. In this case, the optimal cost of the original IK problem is non-zero and need to be determined. To be able to account for such situations we introduce the following alternative rank minimization algorithm.

We define the following function of \mathbf{Y}

$$W(\mathbf{Y}) = \sum_i^{n_r} 3 - \lambda_1(\mathbf{Y}_i) \quad (40)$$

Lemma 3: For any two $\mathbf{Y}^k, \mathbf{Y}^{k+1}$ it holds that

$$W(\mathbf{Y}^{k+1}) \leq W(\mathbf{Y}^k) - \sum_i^{n_r} \langle \nabla \lambda_1(\mathbf{Y}_i^k), \mathbf{Y}_i^{k+1} - \mathbf{Y}_i^k \rangle. \quad (41)$$

Proof: From Lemma 2, we have that $\lambda_1(\mathbf{Y}_i)$ is a convex function of the entries of \mathbf{Y} , hence $3 - \lambda_1(\mathbf{Y}_i)$ is a concave function, and the sum of concave functions is still concave. As a consequence of the properties of concave functions we have

$$W(\mathbf{Y}^{k+1}) \leq W(\mathbf{Y}^k) + \langle \nabla_{\mathbf{Y}^k} W(\mathbf{Y}^k), \mathbf{Y}^{k+1} - \mathbf{Y}^k \rangle. \quad (42)$$

By substituting (40) we can get (41). \blacksquare

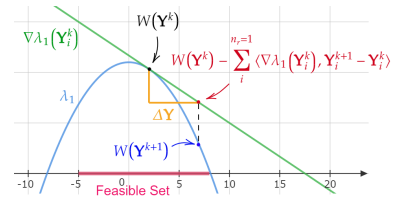


Fig. 4: Suppose $n_r = 1$ and $3 - \lambda_1$ is a concave quadratic function, this figure shows the relation in Lemma 3 resulted from the concavity of the function.

Proposition 9: Given a sequence $\{\mathbf{Y}^k\}$ and a constant c , if the condition

$$W(\mathbf{Y}^k) - \sum_i^{n_r} \langle \nabla \lambda_1(\mathbf{Y}_i^k), \mathbf{Y}_i^{k+1} - \mathbf{Y}_i^k \rangle \leq cW(\mathbf{Y}^k) \quad (43)$$

is satisfied for every k , then

$$W(\mathbf{Y}^k) \leq c^k W(\mathbf{Y}^0) \quad (44)$$

for every k .

Proof: Eq.(43) combined with Lemma 3 implies that $W(\mathbf{Y}^{k+1}) \leq cW(\mathbf{Y}^k)$. The claim then follows by induction. \blacksquare

Theorem 1: If (43) is satisfied for every k and $c \in [0, 1]$, then $\lim_{k \rightarrow \infty} W(\mathbf{Y}^k) = 0$.

Proof: Since $\mathbf{Y}_i^k \succeq 0$ and $\text{tr}(\mathbf{Y}_i^k) = 3$, we have $\lambda_1(\mathbf{Y}_i^k) \leq 3$, and $W(\mathbf{Y}^k) \geq 0$. Combined with Proposition 9

we know that $0 \leq W(\mathbf{Y}^k) \leq 3n_r c^k$. The claim then follows by the squeeze theorem. ■

Equivalently, if we replace \mathbf{Y}_i with \mathbf{Y}_{τ_i} and change 3 into 2 in (40), Theorem 1 also holds because the trace of \mathbf{Y}_{τ_i} is always 2. We develop the following problem to be solved iteratively in the rank minimization process.

Problem 4 (Alternative update problem):

$$\min_{\mathbf{U}^k, \mathbf{U}_\tau^k} f(\mathbf{Y}^{k-1} + \mathbf{U}^k, \mathbf{Y}_\tau^{k-1} + \mathbf{U}_\tau^k) \quad (45a)$$

subject to

$$\sum_{i \in \mathcal{V}_r} \text{vec}(\mathbf{U}_i^k)^\top \nabla \lambda_1(\mathbf{Y}_i^{k-1}) \geq \sum_{i \in \mathcal{V}_r} (c-1)(\lambda_1(\mathbf{Y}_i^{k-1})-3) \quad (45b)$$

$$\sum_{i \in \mathcal{V}_p} \text{vec}(\mathbf{U}_{\tau_i}^{k-1})^\top \nabla \lambda_1(\mathbf{Y}_{\tau_i}^{k-1}) \geq \sum_{i \in \mathcal{V}_p} (c-1)(\lambda_1(\mathbf{Y}_{\tau_i}^k)-2) \quad (45c)$$

$$\mathbf{Y}^{k-1} + \mathbf{U}^k, \mathbf{Y}_\tau^{k-1} + \mathbf{U}_\tau^k \in \bar{\mathcal{Y}} \quad (45d)$$

In the above problem, (45b) and (45c) are derived by substituting $\mathbf{W}(\mathbf{Y})$ and $\mathbf{W}(\mathbf{Y}_\tau)$ into (43), respectively. By enforcing (45b) and (45c) and according to Theorem 1, we have $\lim_{k \rightarrow \infty} \lambda_1(\mathbf{Y}_i^k) = 3, \forall i \in \mathcal{V}_r$ and $\lim_{k \rightarrow \infty} \lambda_1(\mathbf{Y}_{\tau_i}^k) = 2, \forall i \in \mathcal{V}_p$. By updating \mathbf{Y} and \mathbf{Y}_τ iteratively using Problem 4, we can move \mathbf{Y} and \mathbf{Y}_τ toward rank-1 matrices while allowing the cost to increase, thus enabling us to solve for problems where Assumption 1 does not hold. However, in Problem 4 the factor c has to be chosen properly. If c becomes too small, the process becomes too ‘‘aggressive’’ and there might not exist updates \mathbf{U}^k and \mathbf{U}_τ^k such that $\mathbf{Y}^{k-1} + \mathbf{U}^k, \mathbf{Y}_\tau^{k-1} + \mathbf{U}_\tau^k \in \bar{\mathcal{Y}}$. To account for that, we can tune c automatically during the rank minimization process using the following adaptive update of c ,

$$c^+ = 1 - (1 - c)^{p+1}, p = 1, 2, 3, \dots, \quad (46)$$

where c is increased only when the problem becomes infeasible and Problem 4 is solved again using c^+ . Using this adaptive update, we can find a c that is neither too aggressive nor too conservative in terms of increasing λ_1 .

E. Algorithm

The complete algorithm that solves inverse kinematics Problem 1 is summarized in Algorithm 1.

F. Convergence analysis

We provide below a local convergence analysis for the proposed algorithm. We start with the following assumption.

Proposition 10: When Assumption 1 holds, the optimal $\mathbf{Y}^*, \mathbf{Y}_\tau^*$ of Problem 1 is a global minimizer of Problem 2b.

Proof: The solution $\mathbf{Y}^*, \mathbf{Y}_\tau^*$ is a global minimizer of Problem 2b because Problem 2b is convex. ■

Proposition 11: Every globally optimal solution $\mathbf{Y}^*, \mathbf{Y}_\tau^*$ of Problem 2c is also an optimal solution of Problem 2a, and $\{\mathbf{u}^* = g(\mathbf{Y}^*), \boldsymbol{\tau}^* = \{\mathbf{Y}_{\tau_i}^*(7, 7)\}_{i \in \mathcal{V}_p}\} \in \partial \bar{\mathcal{U}}$.

Proof: For a maximizer $\mathbf{Y}^*, \mathbf{Y}_\tau^*$ of Problem 2c, by Proposition 8 it holds that $\mathbf{Y}^*, \mathbf{Y}_\tau^* \in \mathcal{R}_1$ and since $\{\mathbf{Y}^*, \mathbf{Y}_\tau^*\} = \text{argmin}(f(\mathbf{Y}, \mathbf{Y}_\tau))$ it is an optimal solution to

Algorithm 1 Iterative SDP Inverse Kinematics Solver

Input $\mathbf{T}_{goal}, \mathbf{R}_{goal}, \mu, \epsilon_1, \epsilon_2, k_{max}$
Output \mathbf{x}^*

- 1: Solve Problem 2b to get an initial solution $\mathbf{Y}^0, \mathbf{Y}_\tau^0$ and set $k = 1$.
- 2: **while** $(\exists \lambda_1(\mathbf{Y}_i) \leq 3 - \epsilon_1 \parallel \exists \lambda_1(\mathbf{Y}_{\tau_i}) \leq 2 - \epsilon_1) \& \parallel \mathbf{U}^k \parallel_F \geq \epsilon_2 \& k \leq k_{max}$ **do**
- 3: For each \mathbf{Y}_i^{k-1} , compute the largest eigenvalue $\lambda_1(\mathbf{Y}_i)$ and the corresponding normalized eigenvector $\mathbf{V}_i^{k-1, (1)}$. Repeat the same for $\mathbf{Y}_{\tau_j}^{k-1}$ to get $\lambda_1(\mathbf{Y}_{\tau_j})$ and $\mathbf{V}_{\tau_j}^{k-1, (1)}$
- 4: Solve Problem 3 or Problem 4 to get \mathbf{U}^k and \mathbf{U}_τ^k .
- 5: Update $\mathbf{Y}_i^k = \mathbf{Y}_i^{k-1} + \mathbf{U}_i^k$ for all $i \in \mathcal{V}_r$ and update $\mathbf{Y}_{\tau_j}^k = \mathbf{Y}_{\tau_j}^{k-1} + \mathbf{U}_{\tau_j}^k$ for all $j \in \mathcal{V}_p$ and set $k = k + 1$.
- 6: **end while**
- 7: Recover the rotations $\{\mathbf{R}_i\}$ by reshaping $g(\mathbf{Y}^{k-1})$.
- 8: Recover $\{\tau_i | i \in \mathcal{V}_p\}$ from \mathbf{Y}_τ^{k-1} .
- 9: Recover the translations $\{\mathbf{T}_i\}$ using (3) and (11).
- 10: **return** \mathbf{x}^* defined in (2).

Problem 2a. Using Proposition 6 and 7 we have $\{\mathbf{u}^*, \boldsymbol{\tau}^*\} = \text{image}(\bar{\mathcal{Y}} \cap \mathcal{R}_1) = \mathcal{U} \in \partial \bar{\mathcal{U}}$. ■

Proposition 12: When Assumption 1 holds and $\{\mathbf{Y}^k, \mathbf{Y}_\tau^k\}$ is updated using Algorithm 1 with Problem 3 solved in step 4, it holds that $\{\mathbf{Y}^k, \mathbf{Y}_\tau^k\} \rightarrow \{\tilde{\mathbf{Y}}^*, \tilde{\mathbf{Y}}_\tau^*\}$ as $k \rightarrow +\infty$, and $\tilde{\mathbf{u}}^* = g(\tilde{\mathbf{Y}}^*) \in \partial \bar{\mathcal{U}}$, where $\tilde{\mathbf{Y}}^*, \tilde{\mathbf{Y}}_\tau^*$ is a local maximizer of Problem 2c.

Proof: Consider another version of Problem 2c (we refer it as Problem 2d) where the constraint (36b) is replaced with $\nabla f(\mathbf{Y}, \mathbf{Y}_\tau) = \mathbf{0}$. This new constraint can be seen as a convex relaxation of (36b) because $\nabla f(\mathbf{Y}, \mathbf{Y}_\tau) = \mathbf{0}$ implies that $\mathbf{Y}, \mathbf{Y}_\tau$ is the minimizer of the convex function f . By Lemma 2, the objective function of this problem is convex in \mathbf{Y} and \mathbf{Y}_τ , respectively. As a result, Problem 2d is a maximization of a convex function over a convex set. Algorithm 1 can be seen as a gradient approach to Problem 2d. Since $\bar{\mathcal{Y}}$ is bounded, when $k \rightarrow +\infty$, we have $\{\mathbf{u}, \boldsymbol{\tau}\} \rightarrow \{\mathbf{u}^*, \boldsymbol{\tau}^*\} \in \partial \bar{\mathcal{U}}$, where $\mathbf{u}^* = g(\tilde{\mathbf{Y}}^*)$, $\boldsymbol{\tau}^* = \{\tilde{\mathbf{Y}}_{\tau_i}^*(7, 7)\}_{i \in \mathcal{V}_p}$, and $\tilde{\mathbf{Y}}^*, \tilde{\mathbf{Y}}_\tau^*$ is a local maximizer. To see why, for any point $\mathbf{Y}, \mathbf{Y}_\tau$ in the neighborhood $N(\tilde{\mathbf{Y}}^*, \tilde{\mathbf{Y}}_\tau^*)$ such that $\mathbf{Y}, \mathbf{Y}_\tau \in \bar{\mathcal{Y}}$ and $\{\nabla f(\mathbf{Y}) = \mathbf{0}\}$, it holds that $\lambda_1(\tilde{\mathbf{Y}}^*) \geq \lambda_1(\mathbf{Y})$ and $\lambda_1(\tilde{\mathbf{Y}}_\tau^*) \geq \lambda_1(\mathbf{Y}_\tau)$ because by contradiction if there were a $\hat{\mathbf{Y}}, \hat{\mathbf{Y}}_\tau \in N(\tilde{\mathbf{Y}}^*, \tilde{\mathbf{Y}}_\tau^*)$ and $\hat{\mathbf{Y}} = \mathbf{Y}^{k-1} + \hat{\mathbf{U}}_k, \hat{\mathbf{Y}}_\tau = \mathbf{Y}_\tau^{k-1} + \hat{\mathbf{U}}_\tau^k$ such that $\lambda_1(\hat{\mathbf{Y}}) \geq \lambda_1(\tilde{\mathbf{Y}}^*), \lambda_1(\hat{\mathbf{Y}}_\tau) \geq \lambda_1(\tilde{\mathbf{Y}}_\tau^*)$, then the fact that $\{\mathbf{U}^k, \mathbf{U}_\tau^k\}$ is a maximizer of (38a) would not hold. ■

Proposition 13: When Problem 1 is feasible and $\{\mathbf{Y}^k, \mathbf{Y}_\tau^k\}$ is updated using Algorithm 1 with Problem 4 solved in step 4, it holds that $\{\mathbf{Y}^k, \mathbf{Y}_\tau^k\} \rightarrow \{\tilde{\mathbf{Y}}^*, \tilde{\mathbf{Y}}_\tau^*\}$ as $k \rightarrow +\infty$, and $\tilde{\mathbf{u}}^* = g(\tilde{\mathbf{Y}}^*) \in \partial \bar{\mathcal{U}}$, where $\tilde{\mathbf{Y}}^*, \tilde{\mathbf{Y}}_\tau^*$ is a local maximizer of Problem 2c.

Proof: According to Theorem 1, $\lim_{k \rightarrow \infty} W(\mathbf{Y}^k) = \lim_{k \rightarrow \infty} W(\mathbf{Y}_\tau^k) = 0$ when (45b) and (45c) are satisfied, meaning that $\lim_{k \rightarrow \infty} \sum_{i \in \mathcal{V}_r} \lambda_1(\mathbf{Y}_i^k) = 3n_r$ and

$\lim_{k \rightarrow \infty} \sum_{i \in \mathcal{V}_p} \lambda_1(\mathbf{Y}_{\tau i}^k) = 3n_p$. As a result, $\{\tilde{\mathbf{Y}}^*, \tilde{\mathbf{Y}}_{\tau}^*\}$ becomes a maximizer of Problem 2c. It is a local maximizer because for any $\mathbf{Y}, \mathbf{Y}_{\tau}$ in the neighborhood $N(\tilde{\mathbf{Y}}^*, \tilde{\mathbf{Y}}_{\tau}^*)$ that satisfies all the constraints in Problem 4, it holds that $\lambda_1(\tilde{\mathbf{Y}}^*) \geq \lambda_1(\mathbf{Y})$ and $\lambda_1(\tilde{\mathbf{Y}}_{\tau}^*) \geq \lambda_1(\mathbf{Y}_{\tau})$. From Proposition 7 we know that the $\{\mathbf{u}, \boldsymbol{\tau}\} \rightarrow \{\mathbf{u}^*, \boldsymbol{\tau}^*\} \in \partial \bar{\mathcal{U}}$, where $\mathbf{u}^* = g(\tilde{\mathbf{Y}}^*)$, $\boldsymbol{\tau}^* = \{\tilde{\mathbf{Y}}_{\tau i}^*(7, 7)\}_{i \in \mathcal{V}_p}$. ■

VIII. PERFORMANCE IMPROVEMENTS

To improve performance, we introduce some additional modifications to our method.

A. Restart

Because the proposed rank minimization scheme can only guarantee local convergence, it is possible that $\{\mathbf{Y}^k, \mathbf{Y}_{\tau}^k\}$ stops at a solution where the rank is greater than one. We propose an Algorithm 2 to move $\{\mathbf{Y}^k, \mathbf{Y}_{\tau}^k\}$ to another point within the feasible set $\bar{\mathcal{U}}$ and restart rank minimization from there. To begin with, we pick a small positive factor δ .

Algorithm 2 Restart

Input $\mathbf{Y}, \mathbf{Y}_{\tau}, \delta$

Output $\mathbf{Y}', \mathbf{Y}'_{\tau}$

- 1: For a $t > 0$, find matrices $\mathbf{M}, \mathbf{M}_{\tau}$ such that $\mathbf{Y} + t\mathbf{M}, \mathbf{Y}_{\tau} + t\mathbf{M}_{\tau} \in \bar{\mathcal{Y}}$
 - 2: $\mathbf{Y}' \leftarrow \mathbf{Y} + t\mathbf{M}, \mathbf{Y}'_{\tau} \leftarrow \mathbf{Y}_{\tau} + t\mathbf{M}_{\tau}$
 - 3: **while** $\mathbf{Y}', \mathbf{Y}'_{\tau} \in \bar{\mathcal{Y}}$ **do**
 - 4: $\mathbf{Y}' \leftarrow \mathbf{Y}' + \delta\mathbf{M}, \mathbf{Y}'_{\tau} \leftarrow \mathbf{Y}'_{\tau} + \delta\mathbf{M}_{\tau}$.
 - 5: **end while**
-

By Proposition 7, the low-rank solutions \mathbf{Y} are on the boundary of $\bar{\mathcal{U}}$. In Algorithm 2, \mathbf{Y}^k is manipulated to change such that $\mathbf{Y}', \mathbf{Y}'_{\tau} \in \bar{\mathcal{Y}}$ until $\mathbf{Y}' + \delta\mathbf{M} \notin \bar{\mathcal{Y}}$, meaning that the resulting \mathbf{Y}' is close to the boundary. Although there is no guarantee that this algorithm moves $\mathbf{Y}, \mathbf{Y}_{\tau}$ closer to rank-1 matrices, we can use it to find another starting point in the feasible set $\bar{\mathcal{Y}}$ and restart Algorithm 1 from there. In practice, we find that optimal solutions can be found using this restarted process. More details are presented in Section IX-A.

B. Reducing the number of variables using unit quaternions

In this subsection we show that the number of variables defined in VI-B can be reduced using the unit quaternion $\mathbf{q} = [q_r \ q_x \ q_y \ q_z]^T$. We start by defining the following decision variable.

$$\mathbf{Q} = \mathbf{q}\mathbf{q}^T = \begin{bmatrix} q_r^2 & q_r q_x & q_r q_y & q_r q_z \\ * & q_x^2 & q_x q_y & q_x q_z \\ * & * & q_y^2 & q_y q_z \\ * & * & * & q_z^2 \end{bmatrix} \in \mathbb{R}^{4 \times 4} \quad (47)$$

It can be seen that \mathbf{Q} is a rank-1 matrix with fixed trace equals to 1, which allows us to perform the same rank minimization procedure as in Algorithm 1 to recover the rank-1 property.

Moreover, the unit quaternion can be converted to a rotation matrix using the following transformation [22, section 2.6].

$$\mathbf{R}_q = \begin{bmatrix} 1 - 2(q_y^2 + q_z^2) & 2(q_x q_y - q_z q_r) & 2(q_x q_z + q_y q_r) \\ 2(q_x q_y + q_z q_r) & 1 - 2(q_x^2 + q_z^2) & 2(q_y q_z - q_x q_r) \\ 2(q_x q_z - q_y q_r) & 2(q_y q_z + 2q_x q_r) & 1 - 2(q_x^2 + q_y^2) \end{bmatrix} \quad (48)$$

Observe that $\mathbf{R}_q \in \mathbf{SO}(3)$ as a function is linear in \mathbf{Q} , which allows us to replace all the rotations in the IK problem with \mathbf{R}_q as a linear function of \mathbf{Q} . In this way, we can assign a \mathbf{Q}_i for every rotation and write Problem 1 as a function of $\{\mathbf{Q}_i, \mathbf{Y}_{\tau}\}$, reducing the size of variables for each rotation from 7×7 to 4×4 .

IX. SIMULATION RESULTS

A. Dual-arm Baxter

To check if our IK solver can find postures for complicated constraints such as closed kinematic chain and joint limits, the proposed method is implemented on a humanoid dual-arm Rethink Robotics Baxter robot. The robot possesses two arms mounted on a fixed torso. Each arm has 7 revolute joints with angle limits. We model the arms of the robot as one closed kinematic chain by rigidly aligning the two grippers on a common line with a fixed distance to simulate the task of collaboratively holding a box. The objective is to solve for postures of the robot given some predetermined goal poses of the end-effector.

Unlike most traditional IK solvers, which can only deal with open kinematic chains, our solver can evaluate the kinematic chain as a whole without cutting it into separate sub-trees. This can be done by adding a linear constraint discussed in Remark 1 to Problem 2b.

variable type	variable size	number of rows (equality/inequality)
rotations	$\mathbf{Y} \in \mathbb{R}^{7 \times 7n_r}$	137/6112
quaternions	$\mathbf{Q} \in \mathbb{R}^{4 \times 4n_r}$	92/6112

variable type	$err(\mathbf{R}_{ee})$	$err(\mathbf{T}_{ee})$
rotations	$1.59 \cdot 10^{-8}$	$4.61 \cdot 10^{-9}$
quaternions	$1.62 \cdot 10^{-16}$	$9.60 \cdot 10^{-9}$

TABLE I: Problem sizes and results when solving the Dual-arm Baxter example using two different types of variables

The simulation is performed separately, where the IK problem is either formulated as functions of \mathbf{Y} defined with rotations or \mathbf{Q} defined with quaternions. Figure 5 shows a solution to a given \mathbf{T}_{goal} and \mathbf{R}_{goal} using our IK solver. In this example, the total number of free links is $n_r = 15$, which defines the size of the problem shown in Table I. The end-effector is set as the midpoint of the two grippers and is treated as a link of the robot assigned with the reference frame $\{\mathbf{R}_{ee}, \mathbf{T}_{ee}\}$. The errors of the end-effector pose, $err(\mathbf{R}_{ee}) = \|\text{vec}(\mathbf{R}_{ee}) - \text{vec}(\mathbf{R}_{goal})\|_2$ and $err(\mathbf{T}_{ee}) = \|\mathbf{T}_{ee} - \mathbf{T}_{goal}\|_2$ are compared for the two variable selections in Table I. We verified that all the poses satisfy the imposed constraints in Problem 1 along with the translation relation (3). Figure 6 shows some results regarding

the computation process where 6a and 6b show the change of the largest eigenvalue, λ_1 of each \mathbf{Y}_i^k and \mathbf{Q}_i^k during the rank minimization process. We observed that values of λ_1 increase iteratively, eventually reaching the maximum value of 3 (or 1, given by the trace constraint). Figures 6c and 6d present the eigenvalues of every \mathbf{Y}_i in the final solution, where all eigenvalues except λ_1 are below the tolerance ϵ_1 . This shows that each \mathbf{Y}_i and \mathbf{Q}_i in the solution is approximately a rank-1 matrix. With the above results, we can say that in this example, the solver successfully solves the IK problem.

To test the performance of our solver on multiple different targets, we implement it on a set of random end-effector poses. We build this set by randomly sampling 500 points in a space $\mathbf{T}_{goal} = [x, y, z]^T \in \mathcal{T}_{goal}$, where $x \in [0.4, 0.75]$, $y \in [-0.2, 0.2]$, and $z \in [0.2, 0.7]$. For each point, we assign a randomly generated orientation $\mathbf{R}_{goal} = \mathbf{R}_z(\alpha)\mathbf{R}_y(\beta)\mathbf{R}_x(\gamma) \in \mathcal{R}_{goal}$, where $\alpha \in [0, \pi/2]$, $\beta \in [0, \pi]$, and $\gamma \in [\pi/2, 0]$. These poses are selected based on the mutual reachable space of the arms but are not guaranteed to have feasible IK solutions. For comparison, we applied a BFGS IK solver (available with the MATLAB `generalizedInverseKinematics` class) to the same problem set. It is worth-mentioning that this solver can only find solutions to open kinematic chains. Therefore, for a mutual end-effector pose of the two arms, the BFGS solver is applied twice, one for each arm, which is different from our method. Moreover, unlike our method, the BFGS solver requires an initial guess every time, which is set to be the zero joint angles in this simulation. The MOSEK [16] SDP solver is employed to solve the SDP problems within our method. Eventually, the results are visualized in Figure 7, where the sampled goals are colored in terms of which of the methods succeed. In this result we count our method as successful if the problem is solved using any of the two types of variables. It is seen that in the tested 500 problems, in 364 times both methods succeed (72.8%, green dots); in 29 times only our method succeeds (5.8%, blue dots); in 24 times only BFGS succeeds (4.8%, purple dots); and in 83 times both solvers fail (16.6%, red dots). The solvers are compared for their performance in Table II including success rates and for successful solutions: the average time covering only the time consumed in the SDP solver, the total iterations taken in average, and the average errors of the end-effector poses. Some other results of our method are also listed. This includes maximal $\|\mathbf{R}_i - P(\mathbf{R}_i)\|_F$, which is the maximal value of all Frobenius norms of the difference between computed \mathbf{R}_i and its projection $P(\mathbf{R}_i)$ on $\mathbf{SO}(3)$ (see [24]), for all $i \in \mathcal{V}_r$ in the successful solutions. This shows how close to the $\mathbf{SO}(3)$ manifold the computed rotations are. Another result is the maximal value within all of the second largest eigenvalues of every \mathbf{Y}_i in the successful solutions. This shows how close to rank-1 matrix each \mathbf{Y}_i is. The results with different variable types and their overall best performances are listed in Table II.

Looking at the results in Table II, we see that IKSPARK has a similar success rate and precision while computes

results slower than the BFGS solver. Observe that with smaller variable size, results with quaternions show faster speed that is comparable with BFGS. The last two columns of Table II shows that our method finds valid solutions with rank-1 solutions and the recovered rotations are on $\mathbf{SO}(3)$, which verifies that the proposed rank minimization algorithm works. From the results in Figure 7 we see that the proposed method can find solutions in problems that the BFGS solver fails.

To see how the restart algorithm works on situations where the solutions stuck at local convergence, we select a sub-optimal solution where Algorithm 1 stops with the condition $\|\mathbf{U}^k\|_F < \epsilon_2$ and input it into Algorithm 2, from which we obtain another point in the relaxed set. We then minimize the rank of this point using Steps 2-6 in Algorithm 1. The change of eigenvalues over this process of a successful result is shown in Fig. 8. It is seen that at first the rank minimization returns with a set of matrices with higher ranks. Then, the restart process projects these matrices to another point and the solver is able to minimize the rank of this new point to rank-1.

Next, the restart algorithm is applied to the problems above where IKSPARK fails to find a solution, where each problem is given 10 attempts to restart consecutively until success. The results are presented in Table III. It is observed that the restart algorithm can find solutions for some of the previously failed cases in a few attempts.

We then test the solver on a different problem set, where the x values in \mathcal{T}_{goal} above are added by 2. We know that any of the pose in this space is beyond reach of the robot end-effector. We use our solver to test infeasibility of these problems. To do so, for each pose we solve the infeasibility problem constructed by adding all of the constraints in (2b) along with the constraint $\nabla f(\mathbf{Y}, \mathbf{Y}_\tau) = \mathbf{0}$. As a result, the solver detects infeasibility for all of the 500 target poses, which matches our expectation of certifying infeasibility.

To test how the alternative rank minimization technique works on these problem where $\min f(\mathbf{Y}, \mathbf{Y}_\tau) \neq 0$, we input the 500 ‘‘out-of-reach’’ poses to Algorithm 1 with Problem 4 solved in Step 4. The results are listed in Table IV. It is observed that the performance varies when different c values are selected. When c is smaller, the algorithm may converge faster while sometimes the solver fails to find a solution that satisfy (44) in a step. When c becomes larger, more iterations are taken and the cost is observed to have larger increase. Meanwhile, it is seen in more cases when c gets larger that the algorithm stops with little improvements. Finally, the adaptive update technique of c values in (46) is used. It is seen that the success rate is improved with this technique while the average cost increase $\Delta \bar{f}$ tends to be larger.

B. Stewart platform with prismatic joints

We show in this subsection that that our solver can find solutions for robots with prismatic joints. As an example, we implement our solver on a Stewart platform [23], which is a parallel robot with 2 rigid bodies connected by 6 legs. Each leg is a prismatic joint attached with the bodies through spherical joints. We first select a geometrical parameter from

Method	Success rate	Avg. time/iterations	$\overline{err}(\mathbf{R}_{ee})$	$\overline{err}(\mathbf{T}_{ee})$	$\max(\ \mathbf{R}_i - P(\mathbf{R}_i)\ _F)$	maximal e_2
IKSPARK(rotations)	76.6%	1.2629(s)/7.89	$1.030 \cdot 10^{-8}$	$3.7495 \cdot 10^{-9}$	$6.9394 \cdot 10^{-6}$	$6.7919 \cdot 10^{-6}$
IKSPARK(quaternions)	76.4%	0.2889(s)/3.64	$1.4879 \cdot 10^{-16}$	$6.8376 \cdot 10^{-9}$	$2.1187 \cdot 10^{-5}$	$7.5648 \cdot 10^{-8}$
BFGS	77.6%	0.1966 s	$1.3452 \cdot 10^{-8}$	$5.9359 \cdot 10^{-9}$	-	-

TABLE II: Performance of IKSPARK on 500 different goals compared against the BFGS solver

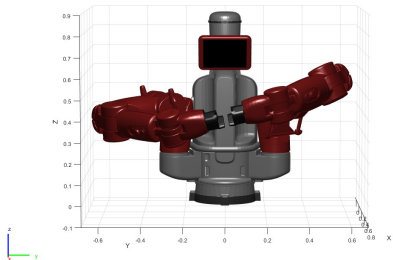


Fig. 5: An example posture solved for Baxter, where the two arms are modeled as one closed kinematic chain.

variable type	Success rate	Avg. attempts	Avg. time/iterations
rotations	16.25%	2.32	11.78(s)/103.8
quaternions	15.58%	2.66	5.12(s)/59.2

TABLE III: The failed results in the 500 poses are given chances to restart using Algorithm 2.

[8], which is used as an example in [19]. The detailed parameters about this robot is listed in Table VI on the left side. For this example, the reference frame for the end-effector is attached rigidly in the center of the top surface and the limits τ_l and τ_u are set as 0.0001 and 1. Then, IKSPARK is implemented for 100 random sampled poses in the space $\mathcal{T}_{goal} := \{\mathbf{T}_{goal} = [x, y, z]^T | x \in [0.2, 0.8], y \in [-0.3, 0.3], z \in [0.8, 1.05]\}$ and $\mathcal{R}_{goal} := \{\mathbf{R}_{goal} = \mathbf{R}_z(\alpha)\mathbf{R}_y(\beta)\mathbf{R}_x(\gamma) | \alpha \in [-\pi/3, \pi/3], \beta \in [-\pi/12, \pi/12], \gamma \in [-\pi/12, \pi/12]\}$. It is observed that our solver is able to find solutions for all of the poses and the average execution time and iterations are 0.2998 seconds and 15.83 steps.

To better check the correctness of the solutions, we then choose another Stewart platform given in [6], the parameters of which is presented in Table VI. This robot has 6 legs with fixed length and is known to have 40 different configurations. With the legs treated as prismatic joints and using the 40 configurations as input, it is expected that the extensions of these prismatic joints match the fixed values. The average difference between the extensions of the solved prismatic joints and the fixed leg length are listed in Table V. It is seen that the computed extensions are very close to the groundtruth values, validating the precision of the IK solutions.

variable type	c	Success rate	Avg. time/iterations	$\Delta \bar{f}$
rotations	0.2	29.6%	0.6429(s)/7.07	+0.0391
quaternions	0.05	62.2%	0.3623(s)/4.41	+0.0342
rotations	0.4	55.0%	0.9548(s)/10.95	+0.0809
quaternions	0.1	80.20%	0.4020(s)/5.07	+0.0521
rotations	0.8	28.8%	3.6441(s)/47.36	+0.1404
quaternions	0.2	67.6%	0.4886(s)/7.06	+0.0607
rotations	adaptive	99.6%	1.6226(s)/7.83	+0.1239
quaternions	adaptive	97.0%	0.5170(s)/5.33	+0.0905

TABLE IV: Performance of IKSPARK solving IK problems for 500 targets where the minimal costs are non-zero.

X. CONCLUSIONS

In this paper we introduce IKSPARK that uses a new relaxation of the feasible sets in the inverse kinematics problem. The relaxed set is convex and contains every feasible solutions, meaning that we can use it to certify infeasibility. We show through simulations that the proposed method is applicable to closed kinematic chain and can serve as an alternative approach for existing solvers. We also show that the solver is capable for robots with prismatic joints.

REFERENCES

- [1] A. Aristidou and J. Lasenby. Fabrik: A fast, iterative solver for the inverse kinematics problem. *Graphical Models*, 73(5):243–260, 2011.
- [2] A. S. Bandeira, N. Boumal, and A. Singer. Tightness of the maximum likelihood semidefinite relaxation for angular synchronization. *Mathematical Programming*, 163:145–167, 2017.
- [3] P. Beeson and B. Ames. Trac-ik: An open-source library for improved solving of generic inverse kinematics. In *2015 IEEE-RAS 15th International Conference on Humanoid Robots (Humanoids)*, pages 928–935, 2015.
- [4] H. Dai, G. Izatt, and R. Tedrake. Global inverse kinematics via mixed-integer convex optimization. *The International Journal of Robotics Research*, 38(12-13):1420–1441, 2019.
- [5] R. Diankov. Automated construction of robotic manipulation programs. 2010.
- [6] P. Dietmaier. The stewart-gough platform of general geometry can have 40 real postures. In *Advances in robot kinematics: Analysis and control*, pages 7–16. Springer, 1998.
- [7] M. Giamou, F. Marić, D. M. Rosen, V. Peretroukhin, N. Roy, I. Petrović, and J. Kelly. Convex iteration for distance-geometric inverse kinematics. *IEEE Robotics and Automation Letters*, 7(2):1952–1959, 2022.
- [8] M. W. Griffiths and J. Duffy. Method and apparatus for controlling geometrically simple parallel mechanisms with distinctive connections, Jan. 12 1993. US Patent 5,179,525.
- [9] M. L. Husty, M. Pfüner, and H.-P. Schröcker. A new and efficient algorithm for the inverse kinematics of a general serial 6r manipulator. *Mechanism and machine theory*, 42(1):66–81, 2007.
- [10] B. Kenwright. Inverse kinematics–cyclic coordinate descent (ccd). *Journal of Graphics Tools*, 16(4):177–217, 2012.
- [11] T. Le Naour, N. Courty, and S. Gibet. Kinematics in the metric space. *Computers & Graphics*, 84:13–23, 2019.

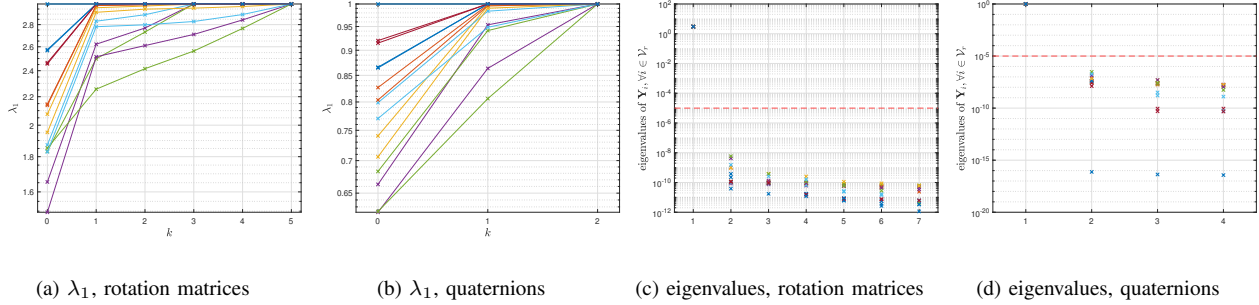


Fig. 6: Some computational results of the solution in Fig. 5. Figures 6a and 6b show the changes of the largest eigenvalues λ_1 of each \mathbf{Y}_i^k and $\mathbf{Q}_{k,i}$ over iteration k when different types of variables are used, where each line corresponds to one matrix. Figures 6c and 6d compare the eigenvalues of each \mathbf{Y}_i and \mathbf{Q}_i in the solution, where all eigenvalues except the largest one are below the tolerance ϵ_1 (red dashed line).

leg#	1	2	3	4	5	6
error	$0.073 \cdot 10^{-6}$	$-0.713 \cdot 10^{-6}$	$0.267 \cdot 10^{-6}$	$-1.048 \cdot 10^{-6}$	$-1.242 \cdot 10^{-6}$	$0.089 \cdot 10^{-6}$

TABLE V: The Stewart platform in [6] is re-modeled with its 6 fixed-length legs replaced with prismatic joints. Above lists the average difference between the solved prismatic joint extensions and the fixed leg lengths when the 40 known configurations are used as goals.

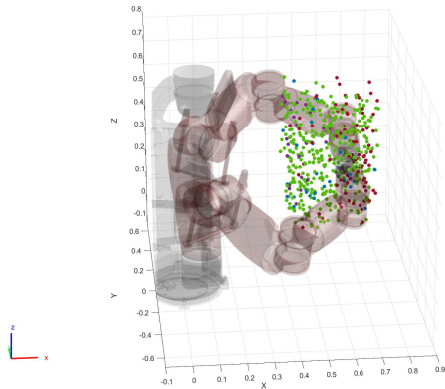


Fig. 7: Implementations of the proposed method and a traditional BFGS Gradient Projection method on a dual-arm Baxter for 500 different end-effector poses with the results: both of the solver succeed (green dots); only our solver succeeds (blue dots); only BFGS succeeds (purple dots); both solvers fail (red dots).

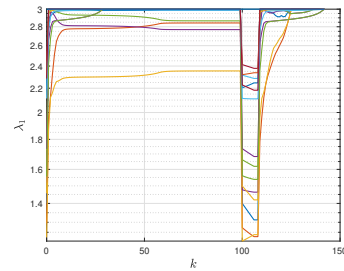


Fig. 8: The change of the largest eigenvalues where a sub-optimal solution from Algorithm 1 ($k = 1, \dots, 100$) is projected to another point in the relaxed set using Algorithm 2 ($k = 101, \dots, 108$) and restarted again with Algorithm 1 ($k = 109, \dots, 142$).

[12] H.-Y. Lee and C.-G. Liang. Displacement analysis of the general spatial 7-link 7r mechanism. *Mechanism and machine theory*, 23(3):219–226, 1988.

[13] M. Li, G. Liang, H. Luo, H. Qian, and T. L. Lam. Robot-to-robot relative pose estimation based on semidefinite relaxation optimization. In *International Conference on Intelligent Robots and Systems (IROS)*, pages 4491–4498, 2020.

[14] J. R. Magnus. On differentiating eigenvalues and eigenvectors. *Econometric Theory*, 1:179–191, 1985.

[15] F. Marić, M. Giamou, A. W. Hall, S. Khoubyarian, I. Petrović, and J. Kelly. Riemannian optimization for distance-geometric inverse kinematics. *IEEE Transactions on Robotics*, 38(3):1703–1722, 2021.

[16] MOSEK ApS. *The MOSEK optimization toolbox for MATLAB manual. Version 10.0.*, 2022.

[17] R. Muller-Cajar and R. Mukundan. Triangulation—a new algorithm for inverse kinematics, 2007.

[18] L. Peng, M. Fazlyab, and R. Vidal. Semidefinite relaxations of Truncated Least-Squares in robust rotation search: Tight or not. In *European Conference on Computer Vision (ECCV)*, 2022.

[19] J. M. Porta, L. Ros, and F. Thomas. A linear relaxation technique for the position analysis of multiloop linkages. *IEEE Transactions on Robotics*, 25(2):225–239, 2009.

[20] M. Raghavan and B. Roth. Inverse kinematics of the general 6r manipulator and related linkages. 1993.

[21] J. Saunderson, P. A. Parrilo, and A. S. Willsky. Semidefinite descriptions of the convex hull of rotation matrices. *SIAM Journal on Optimization*, 25(3):1314–1343, 2015.

[22] B. Siciliano, L. Sciacivco, L. Villani, and G. Oriolo. Modelling, planning and control. *Advanced Textbooks in Control and Signal Processing*. Springer, 2009.

[23] D. Stewart. A platform with six degrees of freedom. proceedings of the institute of mechanical engineers. 1965.

[24] S. Umeyama. Least-squares estimation of transformation parameters between two point patterns. *IEEE Transactions on Pattern Analysis & Machine Intelligence*, 13(04):376–380, 1991.

- [25] L. Wu and R. Tron. An sdp optimization formulation for the inverse kinematics problem. In *2023 62nd IEEE Conference on Decision and Control (CDC)*, pages 4731–4738, 2023.
- [26] H. Yang. *Certifiable Outlier-Robust Geometric Perception*. PhD thesis, Massachusetts Institute of Technology, 2022.
- [27] H. Yang and L. Carlone. A quaternion-based certifiably optimal solution to the Wahba problem with outliers. In *International Conference on Computer Vision (ICCV)*, pages 1665–1674, 2019.
- [28] H. Yang, J. Shi, and L. Carlone. TEASER: Fast and certifiable point cloud registration. *IEEE Transactions on Robotics*, 37(2):314–333, 2020.
- [29] T. Yenamandra, F. Bernard, J. Wang, F. Mueller, and C. Theobalt. Convex optimisation for inverse kinematics. In *2019 International Conference on 3D Vision (3DV)*, pages 318–327. IEEE, 2019.

APPENDIX I

SEPARATE PROOF FOR PROPOSITION 3

In this appendix we provide a separate proof of the claim in Proposition 3 that any rank-1 \mathbf{Y}_{τ_i} satisfying (24) can be written as

$$\mathbf{Y}_{\tau_i} = \begin{bmatrix} \sqrt{t}\mathbf{y}_1 \\ \sqrt{(1-t)}\mathbf{y}_1 \\ \pm\sqrt{t} \\ \pm\sqrt{1-t} \end{bmatrix} \begin{bmatrix} \sqrt{t}\mathbf{y}_1 \\ \sqrt{(1-t)}\mathbf{y}_1 \\ \pm\sqrt{t} \\ \pm\sqrt{1-t} \end{bmatrix}^T, \quad (49)$$

where $\text{tr}(\mathbf{y}_1\mathbf{y}_1^T) = 1$, $t \in [0, 1]$ and the “ \pm ”s in the last two entries of the multiplier vector take the same sign. To begin with, for any vector $\tilde{\mathbf{y}} \neq \mathbf{0} \in \mathbb{R}^n$ we can write $\tilde{\mathbf{y}}\tilde{\mathbf{y}}^T = a\mathbf{y}\mathbf{y}^T$, where $a > 0$ and \mathbf{y} is a unit vector. Then we can write any rank-1 \mathbf{Y}_{τ_i} in the form

$$\mathbf{Y}_{\tau_i} = \begin{bmatrix} a\mathbf{y}_1 \\ b\mathbf{y}_2 \\ c \\ d \end{bmatrix} \begin{bmatrix} a\mathbf{y}_1 \\ b\mathbf{y}_2 \\ c \\ d \end{bmatrix}^T, \quad a, b > 0, \text{ and} \quad (50)$$

$$\|\mathbf{y}_1\| = \|\mathbf{y}_2\| = 1. \quad (51)$$

From constraint 2) in (24), we have $a^2 \text{tr}(\mathbf{y}_1\mathbf{y}_1^T) = a^2 = c^2$ and $b^2 \text{tr}(\mathbf{y}_2\mathbf{y}_2^T) = b^2 = d^2$. Substitute these relations in 1) we have $c^2 + d^2 = 1$. We then let $c^2 = t$ and by 5) we have $t \in [0, 1]$ thus $a^2 = t$ and $b^2 = d^2 = 1 - t$. The constraints 4) and 6) restricts that $ab = cd \geq 0$. By multiplying ac on both side we have $a^2bc = c^2ad$ and $bc = ad$. By the constraint 3) we know that $bcy_2 = ady_1$ and therefore $\mathbf{y}_1 = \mathbf{y}_2$. Because $cd \geq 0$ there exists two cases where whether $c = \sqrt{t}$ and $d = \sqrt{1-t}$ or $c = -\sqrt{t}$ and $d = -\sqrt{1-t}$.

TABLE VI: Geometric parameters of the Stewart platforms

i	Griffis/Duffy		A_i	Dietmeier	l_i
	A_i	B_i		B_i	
1	(0, 0, 0)	(0, 0, 0)	(0, 0, 0)	(0, 0, 0)	1
2	(c, s, 0)	(-c, s, 0)	(1.107915, 0, 0)	(0.542805, 0, 0)	0.645275
3	(2c, 2s, 0)	(c, s, 0)	(0.549094, 0.756063, 0)	(0.956919, -0.528915, 0)	1.086284
4	(1 + c, s, 0)	(3c, s, 0)	(0.735077, -0.223935, 0.525991)	(0.665885, -0.353482, 1.402538)	1.503439
5	(2, 0, 0)	(2c, 0, 0)	(0.514188, -0.526063, -0.368418)	(0.478359, 1.158742, 0.107672)	1.281933
6	(1, 0, 0)	(c, -s, 0)	(0.590473, 0.094733, -0.205018)	(-0.137087, -0.235121, 0.353913)	0.771071

The parameters $c = \cos(\pi/3)$ and $s = \sin(\pi/3)$.